Report Prepared by :

H. Wang
A. A. Sagüés

CORROSION OF POST-TENSIONING STRANDS

Contract No. BC353 RPWO#33

Final Report to Florida Department of Transportation

A. A. Sagüés
Principal Investigator
Department of Civil and Environmental Engineering

University of South Florida
Tampa, FL, 33620
November 1, 2005

Technical Report Documentation Page

1. Report No.	2. Government Accession No.	3. Recipient's Catalog No.
BC353 - 33		

4. Title and Subtitle	5. Report Date
CORROSION OF POST-TENSIONING STRANDS	November 1, 2005
	6. Performing Organization Code

7. Author(s)	8. Performing Organization Report No.
H. Wang, A. A. Sagüés	

9. Performing Organization Name and Address	10. Work Unit No. (TRAIS)
Department of Civil and Environmental Engineering University of South Florida Tampa, FL 33620	11. Contract or Grant No. BC353 - 33

12. Sponsoring Agency Name and Address	13. Type of Report and Period Covered
Florida Department of Transportation 605 Suwannee St. MS 30 Tallahassee, Florida 32399 (850)414-4615	Final Report 11/02/01 - 4/30/2005
	14. Sponsoring Agency Code

15. Supplementary Notes

Prepared in cooperation with the USDOT and FHWA

16. Abstract

The objective of this investigation was to identify mechanisms for severe corrosion observed in post tensioned tendons of segmental bridges in Florida. Emphasis was given to long term conditions in bleed water voids. Commercial ductile iron post-tension anchorage assemblies housing unstressed high strength strand, two types of grout and simulated grout voids were subject to simulated water intrusion events with fresh and salty (0.01N NaCl) water. Galvanic current, strand-anchor conductance and potentials were monitored to identify corrosion location and magnitude. The results showed that external water intrusion can be an important contributor to corrosion tendon failure. Conditions for strand steel depassivation can develop even if only modest carbonation of the grout occurs. Fresh water could initiate corrosion if the native chloride content of the grout exceeded a relatively small amount (e.g. 600 ppm). Currently allowable chloride limits for grouting materials may need revision. Galvanic coupling between strand steel and anchorage iron could significantly aggravate corrosion of the strands. Significant corrosion of strands in the void space was observed, especially in a grout that supported high internal relative humidity. Projections of the combined effects of the deterioration mechanisms identified were consistent with the observation of tendon failures in the field after as little as 7 years.

A mathematical model for a simple grout-strand system was proposed and dimensionless equations were formulated to solve the combined polarization and oxygen transport problem. Measurements of oxygen reduction on strand steel in high pH electrolytes and time evolution of electrical resistivity of 5, low-bleed commercial grouts were conducted to obtain model input parameters. Within the range of validity of the model assumptions, simplified computations indicated that oxygen availability was a key factor in determining corrosion severity while grout resistivity was secondary but still important. Predicted corrosion rates were in general agreement with field and laboratory observations. Issues for subsequent model development were identified.

17. Key Words	18. Distribution Statement
Post-tensioning, strand, grout, anchorage, oxygen diffusivity, resistivity	No Restriction This report is available to the public through the NTIS, Springfield, VA 22161

19. Security Classif. (of this report)	20. Security Classif. (of this page)	21. No. of Pages	22. Price
Unclassified	Unclassified	47	

Form DOT F 1700.7 (8-72) Reproduction of completed page authorized

TABLE OF CONTENTS

NOTICE

ACKNOWLEDGMENT

The technical work presented here was in large part conducted cooperatively with R.G. Powers of the Corrosion Laboratory of the Materials Office, Florida Department of Transportation. Part of the material in this report is adapted from prior publications (in particular [Sagüés, 2003] and [Wang, 2005]) that the authors have prepared to disseminate findings obtained under this contract.

EXECUTIVE SUMMARY

Severe corrosion distress and instances of complete failure of external PT were observed in recent years in tendons of pillars or superstructures of three Florida pre-cast segmental bridges over salt water. As PT tendons are critical to the integrity of these structures, this investigation sought to determine the operating corrosion mechanism to support the rational development of corrosion control measures in new and existing FDOT structures . The available evidence suggests that the key deterioration factor was the formation of large bleed water grout voids at or near the anchorages. After initial stages with free bleed water present, the region where the steel emerges from the grout-void interface may be particularly vulnerable because of a combination of detrimental factors including lowered pH of the grout pore water by carbonation from atmospheric carbon dioxide, evaporative local chloride ion enrichment, and adverse galvanic coupling with the rest of the metallic tendon assembly.

The objectives of this work were to evaluate the validity of the corrosion mechanism suggested above, and to develop a predictive model of the corrosion rate of PT steel based on properties of the system that may be quantified by measurement. Such prediction could then be applied to the selection of optimal grout properties and construction methods to minimize deterioration in future construction, and to appropriate preventive rehabilitation of existing structures.

The results showed that conditions leading to strand steel depassivation can develop in anchorages with grout voids if openings to the exterior allow for even modest carbonation of the grout and periodic water intrusion. Fresh water could initiate corrosion if the native chloride content of the grout exceeds a relatively small amount (e.g. 600 ppm). Currently allowable chloride limits for grout materials may need revision. Galvanic coupling between strand steel and anchorage iron was found to have the potential to significantly aggravate corrosion of the strands. Corrosion of strands in the void space can be considerable, especially in grouts that support a high internal relative humidity. Projections of the combined effects of the deterioration mechanisms identified here are consistent with the observation of tendon failures after as little as a few years of service. Practical methodologies were implemented for the

characterization of supplemental grout properties important to corrosion control, such as resistivity and internal relative humidity.

A simplified mathematical model of a corroding strand bundle was formulated, incorporating both polarization and oxygen transport behavior. This initial computational study indicated that oxygen availability is a key factor in determining corrosion severity. Grout resistivity was a secondary but still important factor within the range of validity of the model assumptions. Predicted corrosion rates were in general agreement with field and laboratory observations. Issues for subsequent model development were identified.

INTRODUCTION

In post-tensioning (PT) of concrete a compressive force is applied by stressing tendons (or bars) after the concrete is cast and cured so that deflection and cracking are minimal, even at full load. Severe corrosion distress and even complete failure of external PT was observed in recent years in tendons of pillars or superstructure of three Florida pre-cast segmental bridges over salt water. As PT tendons are critical to the integrity of these structures, this investigation sought to determine the operating corrosion mechanism to support the rational development of corrosion control measures in new and existing FDOT structures .

The first reported incident was at the 18-year old Niles Channel Bridge in the Florida Keys [Powers, 1999, Sagüés, 2000] followed by the 7-year old Mid Bay Bridge (MBB) in the Western panhandle [Corven, 2001] and the 15-year old Sunshine Skyway Bridge over Tampa Bay [FDOT, 2002]. In those structures, the tendons are a bundle of typically 19 or more seven-wire high-strength (ultimate tensile strength 1.86 GPa (270 ksi)) steel strands, contained for much of the length (including the part of the tendon that is external to the concrete) in a high-density polyethylene (HDPE) duct. The tendon terminates at anchorage assemblies (Figure 1) that transfer the longitudinal tendon force to the concrete. Portions of the tendon pass through pipes in intermediate deviation blocks or U-bends to provide lateral force transfer where needed. After tensioning the entire space between tendon and ducts or anchorage is pumped full with a cementitious grout. The grout is intended for corrosion protection of the steel by providing a highly alkaline environment, and also to allow for some force transfer between strand and anchorage in case of strand breakage or loosening.

The observed damage consisted, in each of the three bridges, of one completely separated tendon plus one to several partially detensioned tendons. The completely separated tendons had failed in the anchorage region following severe corrosion of many of the strands, as illustrated in Figure 2. Mechanical failure appears to be the result of simple overload due to locally reduced cross-section, usually in the form of generalized corrosion along several cm with occasional pitting. In the partially detensioned tendons severe corrosion and mechanical failure had affected some but not all of the strands. In one instance the area of severe corrosion was about 2-3 m away from the anchorage. All cases of severe corrosion were associated with large voids where grout was absent. Significant chloride contamination of the remaining grout was observed at the corroded regions. In nearly all cases the affected anchorages were at bridge expansion joints, or underneath horizontal surfaces, where salt and moisture availability was significant. Additionally, HDPE duct cracks were commonly encountered in MBB. Corrosion was not unique to any particular anchorage manufacturer.

The available evidence suggests that the key deterioration factor was the formation of large grout voids at or near the anchorages. The most likely cause of voids is the development of large amounts of bleed water during the grouting process of the materials used for grouting at the time of construction of the affected bridges [Ghorbanpoor, 1993, Powers, 2002]. Bleeding is assisted by wicking of water along the strands and vibration resulting from the grout pumping operations. The bleed water may be subsequently reabsorbed into the grout or lost by evaporation through incomplete anchorage sealing that may result from deficiencies at the pour back on the wedge plate, or elsewhere (e.g. duct connections or duct cracking). Thus, some of the steel is not in contact with the protective highly alkaline grout that is intended to promote passivity of the steel surface. The region where the steel emerges from the grout-void interface may be particularly vulnerable because of a combination of detrimental factors. The

pH of the grout pore water there could be lowered by carbonation from atmospheric carbon dioxide [Moreno, 1998]. At the same time evaporative local chloride ion enrichment may occur, elevating the chloride content (that could be either the small native content of the grout or some larger amount from external contamination) to a level sufficient to cause passivity breakdown at the local pH and potential conditions [Li, 2001, Moreno, 1998]. After corrosion initiation there, aggravation may result from galvanic coupling of the relatively small active region with a larger passive surface consisting of the rest of the strand assembly in the grout, plus other metallic regions of the anchorage such as its cast iron body. Additional local acidification, as it takes place in many localized corrosion processes [Fontana, 1985, Jones 1996] is expected to place at the anode by hydrolysis induced by the presence of the released metal ions. In the absence of free bleed water, the extent of the corrosion macrocell action is expected to depend on the polarization characteristics of the anodic and cathodic zones involved, and on the resistivity of the intervening hardened grout. The corrosion scenario described above has been supported by preliminary laboratory experiments that showed lowered pH and enhanced chloride content (as well as increased grout porosity) at the grout-void interface of a model anchorage assembly [Powers, 2002]. Adverse galvanic coupling with the anchorage and severe active corrosion were documented for that region. The local corrosion rates were on the order of 10^2 $\mu A/cm^2$, sufficient to cause mechanical failure of at least some wires after short periods, e.g. 1 year. Fast corrosion failure of an experimental anchorage has been also reported elsewhere [Tabatabai, 1995]. These cases suggest that some of the damage in the affected bridges may have been already quite advanced early during the service life of the affected bridges.

The present report addresses the above mechanistic issues and summarizes and expands work [Sagüés 2003, Wang, 2005] performed to that end under FDOT sponsorship following upon the initial investigation by Powers [Powers, 2002]. It is noted that a recent investigation sponsored by the Portland Cement Association [Bricker, 2005] presents complementary information in general agreement with many of the findings detailed here.

OBJECTIVE

The objective of this investigation is to evaluate the validity of the corrosion mechanism suggested above, leading to a predictive model of the corrosion rate of PT steel based on properties of the system that may be quantified by measurement. Such prediction could then be applied to the selection of optimal grout properties and construction methods to minimize deterioration in future construction, and to appropriate preventive rehabilitation of existing structures.

APPROACH

To achieve the above objectives, experiments were conducted to elucidate the causes of steel depassivation in PT assemblies, the location of the corrosion, the extent of aggravating corrosion macrocell effects, and the amount and timing of corrosion in the life of the structure. To that end, long term experiments were conducted with multiple mock-up anchor assemblies with a simulated void, partially filled with a plain cement and a commercial grout, and subject to periodic simulated recharge events with fresh and chloride-contaminated water.

Additional experiments were conducted to determine candidate grout materials properties important to corrosion development such as electric resistivity, internal relative

humidity (RH), porosity and pore water pH, and to obtain information on the polarization behavior of PT steel. The results of the experiments were used to formulate a predictive model of corrosion severity in tendons with partially voided anchorages.

EXPERIMENTAL METHODOLOGY

Mock-up Anchor Assemblies

Two series of similarly configured mock-up PT anchorage assemblies (7 total) were constructed using actual anchorage bodies and PT strand. Figures 3a and 3b and Tables 1 to 3 detail configuration details and other system properties.. Series P (assemblies P1 to P3) used a plain cement grout with addition of a commercial, aluminum based expansion agent similar to the grout identified as PN in the next section " Grout Properties and Steel Polarization". This grout represented materials used in earlier construction practice which were found to cause bleed water voids. Series S (S1 to S4) used a new-generation commercial low-bleed grout representative of materials used at present (this grout is from a different batch but otherwise the same product as that designated "A" in the next Section. Unless otherwise indicated the grouts were prepared using de-ionized water and mixed in 5 gallon buckets using a “Jiffy” paddle at ~2500 rpm per procedure suggested by the commercial grout manufacturer and described in more detail in the next subsection. The three Series P assemblies were fastened together on a FMC Syntron VP86C1^{TM} vibrating table operated at its lowest power setting continuously for four hours after casting the grout, simulating vibration that may be encountered in field operations and that may induce bleed water formation. In these assemblies the grout expanded ~5 cm near the top of the assembly and resulted in a ~1.5 cm deep bleed water accumulation on the upper surface that was absorbed/evaporated during the next 2 to 10 days after casting (Table 3). Prior tests showed that no significant bleed water accumulation developed on the A grout upon vibration, so the S-assemblies were not vibrated and, as expected, showed no visible bleed water accumulation.

The anchorage body was made of ductile iron per ASTM A27, Grade 65-45-12 and was attached to a high density polyethylene plastic trumpet. The post-tensioning strands received from a commercial supplier were seven-wire, 15.24mm (0.6″) nominal strand diameter, low relaxation, Grade 1860 per ASTM A416/A416M-98. All the metal components used in the experiments were in “as-received” condition with no signs of preexisting deterioration or contamination. Alloy compositions (Table 2) and microstructures were verified by spectrographic analysis and metallographic examination. Figure 4 shows an optical metallograph of the spheroidal graphite nodules of a ductile cast iron anchor body used in prior work [Powers 2002]. Figure 5 shows Scanning Electron Microscope (SEM) metallographic cross sections of the nearly eutectoid, fine pearlitic microstructure of the high strength PT wires. Consistent with previous reports [Proverbio, 2002; Krumbach, 1998; Enos, 1997; Toribio,1997; Preston, 1990], ferrite and cementite lamellae are aligned with the axis of wire reflecting the cold drawing manufacturing process. Figure 5(a) reveals the thin layer of oxide mill scale, typically 3 to 10μ thick, present in the wires.

The assemblies were set up vertically. An unstressed 7-strand bundle was placed along the center. A full-length counter electrode (CE) made out of mixed-metal oxide activated Ti wire, and embedded reference electrodes (RE) of the same material [Castro, 1996] were placed as shown in Figure 3a, carefully avoiding short circuits. The wire REs were placed

~0.5cm from the strand surface and were intended for short term polarization resistance and Electrochemical Impedance Spectroscopy (EIS) measurements. Absolute potential measurements were performed periodically using a Saturated Calomel Electrode (SCE) placed temporarily against the plastic Luggin-style [Jones, 1996] potential measuring ports having a sensing tip next to the embedded REs. To control evaporative water loss, an inverted glass bowl was sealed on top of the anchor and contact with the external air (typically at 65% RH) was permitted only through the grout vent hole (~5 cm^2) on the side of the anchor body. This arrangement was intended to simulate imperfect sealing in an assembly in the field. The opening did not promote excessive drying, as shown by the observation of fogging of the bowl for periods of days-weeks after simulated wetting incidents in the P assemblies.

Assuming that only the outer surface of strand bundle contacted with the grout, the nominal surface area of anchor steel and strands bundle that was completely immersed in the grout was then calculated to be approximately 760 cm^2 and 1280 cm^2, respectively.

Due to some shrinkage of S grout, thin separation gaps were found at the grout-anchor body interface in all three S assemblies and leaks of recharge water through these gaps were observed. Narrow inter-strand voids were noticed below the level of the bulk grout surface in the S (but not in the P) assemblies (#11, Figure 3). Those inter-strand voids extended for 0.5 to 4 inches as determined by inserting thin (~0.5 mm diameter) wires.

Recharge water events simulating the effects of leaks in an anchor sealing were conducted periodically with fresh water (S series) and both fresh and 0.01N NaCl-contaminated water (S series) as shown in Table 3. The anchor and plastic trumpet were screwed together using built-in spiral threads. The outer circumferential joints (#13, Figure 3) were not sealed to the exterior. For all S series assemblies (and to a much lesser extent in the P series), it was initially noticed that some recharge water flowed immediately out from those joints. All joints were silicone-sealed at day 252 and 138 for the P and S series respectively. Water recharges were repeated when the system reached a relatively steady state or repassivated from previous recharge event. pH paper was used to monitor the pH of any residual recharge water that remained on the top of the grout surface.

The anchor body and the strand bundle were normally electrically connected through a closed external switch allowing macrocell current to flow. Periodically a 0.1 Ω input resistance ammeter or a 97 Hz ac soil resistance meter were inserted across the momentarily opened switch, to monitor the anchor/strand bundle galvanic current or the intervening grout resistance respectively. The potential of the interconnected assembly with respect to a reference electrode placed in the various electrode ports was monitored as well. In a supplementary investigation, linear polarization resistance (LPR) and (EIS) measurements of the interconnected assembly were conducted periodically at the composite mixed potential, sending the excitation current through the full length CE . The results of that portion of the work will be reported elsewhere.

Grout Properties and Steel Polarization

Five commercial grouts (designated A-E) from the Florida Department of Transportation FDOT qualified product list [Harkins, 2002] and a Type 1 plain cement paste were evaluated. The commercial grouts are newly formulated products yielding virtually no bleed water under standard test conditions. The water/grout (W/G) ratios used were between

0.23 and 0.32 for grouts A-E and followed generally recommended practices for those products. The water/cement ratio (W/C) for the paste was 0.45. Values used for individual specimens are noted in the results listings or figures. The plain cement paste (designated as "P") was prepared normally without admixtures, but for some tests it included 1% by wt. of cement of Intraplast-N aluminum-based expanding agent (designated as "PN"). About 7-kg grout/paste and the correspondent amount of tap water (initially at ~22 ^{o}C) were mechanically mixed with a stirring paddle at ~2500 rpm in a 5-gallon bucket per manufacturer's recommendations. Immediately after mixing, a flow fluidity test (Modified ASTM C939) was conducted to verify that an efflux time between 9s and 20s was achieved for commercial grouts.

A wick-induced bleed water test per ASTM C940 was also conducted to measure the amount of water that accumulated on the top of a 1000 mL graduated cylinder. The grout was then cast into plastic cylinder molds usually 10.2 cm (4 inch) long and 5.1 cm (2 inch) diameter. The top of the molds was sealed with flexible paraffin film; The cylinders were broken up and the grout inside used for chloride content tests ~6 months after casting. For grout resistivity tests the cylinders were fitted with 4 metallic contacts spaced ~2.5 cm apart in a row along the side forming a Wenner array. Measurements of electrical resistance were performed periodically with a Nilsson® Model 400 soil resistivity meter and the resistivity was obtained by applying a correction factor [Morris, 1996]. The cylinders were kept sealed tight and evaporation loss was negligible as indicated by periodic weight measurements.

For RH tests the grout was cast into ~4cm diameter, ~ 10 cm long polyethylene containers leaving a ~5 cm long void near one end, which had a 1 cm diameter opening normally airtight sealed by and O-ring and a stopper. Periodically the O-ring was opened and a Vaisala RH probe was temporarily inserted airtight instead of the stopper, and typically allowed to stabilize in the air space overnight. The terminal probe reading was recorded as the RH for that sampling event. The RH probe was periodically calibrated against the airspace of standard RH water-salt solutions.

For pore water pH measurements the grout was cast into duplicate cylinders similar to those used for resistivity tests, and cured in the sealed cylinders for ~6 days. The cylinders were then demolded and placed in a 100% RH chamber for one month, after which ~4mm diameter cavities were drilled on the sides of the cylinders to perform In Situ Leaching (ISL) pore water pH tests keeping the specimens in the 100% RH chamber (Figure 5d) and following procedures detailed by Sagüés [1997]. Cavity water stabilization time was >100 days.

The resistance of grouts to carbonation from exposure to naturally existing CO_2 in air (typically ~300 ppm) was evaluated in exploratory tests with cylindrical specimens 5.1 cm diameter and 10.2 cm long cast as indicated above and mold cured for ~30 days. The cylinders were then demolded and kept separated from each other and exposed to laboratory air (typically 65% RH) and temperature conditions for 138 days. The specimens were then cracked open longitudinally so the crack plane contained the axis of the cylinder. The freshly exposed concrete surface was finely sprayed with a solution of 1% phenolphthalein in methanol, which revealed the carbonated zones. The carbonation front shape (uniform or localized) and its typical depth was noted for the center of the cylinder top and bottom faces, as well as for the perimeter of the cylinder girding its center. From the depth of carbonation x and the time of exposure t a carbonation coefficient $k = x\, t^{-1/2}$ [Moreno 1998] was calculated for each case treating the carbonation front as a flat front as a first approximation. All the

laboratory exposure tests were performed at room temperature, 21±2°C. Grout porosity tests following generally ASTM C642 were conducted on the commercial grouts and on the PN grout after ~10 month and ~5 month curing respectively.

For steel polarization tests, wires 0.5 cm diameter, ~15 cm long and in the as-received mill finish condition were removed from a fresh roll of 1.5 cm, 1.86 GPa (0.6 inch, 270 ksi) A416 PT strands and used to determine their cathodic polarization behavior. The electrolytes used were saturated $Ca(OH)_2$ solution (SCS), simulated pore solution (SPS) and commercial grout. The SCS was prepared by adding 2 g/l $Ca(OH)_2$ to distilled water resulting in pH~12.6. The SPS had 2 g/l $Ca(OH)_2$, 3.70 g/l NaOH, and 10.5 g/l KOH; pH~13.3. Both the cut end of wires in the electrolyte and the region across the electrolyte/air interface were covered with a 2-component epoxy to expose only the side surface and avoid waterline corrosion. An activated titanium rod (ATR) electrode [Li, 2001, Castro, 1996] calibrated against a saturated calomel electrode (SCE) before and after the tests was used as the reference electrode, while a graphite rod was the counter electrode. All tests were performed at room temperature, 21±2°C, and under naturally aerated conditions.

EXPERIMENTAL FINDINGS

Mock-up Assemblies

Visual Symptoms of Corrosion: Figure 6 illustrates the surface condition of the strand bundles in the P assemblies (plain cement) after 308 days when the P1 assembly had only one fresh water recharge and P2 and P3 had one fresh water recharge and two 0.01N NaCl recharges. There was significant variability (days to months) from assembly to assembly in the length of time recharge water was retained at the surface after a recharge event, partly reflecting differences in the gaps in the anchor body-grout interface. P3 had the greatest downward leakage there; in contrast P2 retained 1-2 mm of water at the surface long after the 3rd recharge event as shown in the picture. The picture shows also variability in the amount of grout residue (from bleed water) at the steel surface. There was conspicuous corrosion damage in the air space of the strand bundles of all three P assemblies. That air space corrosion was actually more notable than the rust at the air-grout interface in the P2 and P3 assemblies even after they had experienced some salt water additions. Air space corrosion was however less noticeable in the portion of the strand covered by residual grout, especially in the thicker grout coverage portions of strands in P1.

Figure 7 illustrates the surface condition of the strands in the S assemblies at day 272. These (except for S2 which was a control with no recharge events) were exposed to fresh water events only. There was nevertheless severe air space corrosion at some spots, as well as corrosion attack at the grout/void interface, although not as severe as in the P assemblies. Control assembly S2, which had no water additions, showed no signs of significant corrosion.

Figure 8 illustrates the surface condition of the anchor body ductile iron in P2 and S1 after respective water recharges, showing severe water line corrosion in both. There was some air space corrosion in the P assembly but much less in the S assembly. This may reflect the combined effect of the narrow grout-anchor gap in the S assembly, allowing for faster

water drainage, and lower internal RH (~80%) from self-desiccation of the S grout (discussed next section).

The narrow grout-anchor gap in the S assemblies might have affected corrosion of the strands in various ways. These include increasing the electrical resistance between anchor and strands thus decreasing galvanic current, or conversely allowing faster water penetration down to the locations away from the grout/void interface and then initiate corrosion at those locations. Oxygen, necessary for the cathodic reaction, would also be more easily transported along the opening thus possibly increasing the overall macrocell current for localized corrosion of stands at the grout/void interface [Sagüés, 2003; Powers, 2001] as discussed in the Modeling section.

Electrochemical Observations: Figure 9 shows the anchor/strands galvanic current in the P series assemblies. The arrows indicate water recharge events per Table 3. Positive values denote net anode character for the strands. These were initially strongly anodic (current ~ 500 μA) immediately following initial interconnection, but the current dropped to <10 μA after a few days-weeks likely reflecting maturing passivity of the assembly in the alkaline grout environment.

The first recharge (fresh water, all three P assemblies) caused only small transient changes in galvanic current. Visual inspection shortly afterwards showed no rust on the strands at the grout/void interface. Galvanic current was small in the following 4-month waiting period. Addition of NaCl-spiked recharge water into P2 and P3 at days 179 and 245 caused sharp transient increases (to 1000 μA) in macrocell current, but with the strands acting as net cathodes. However, in the next salt water recharge event (day 320, all three assemblies) the strands in P3 became anodic and slight yellow or brown rusting was noticed on those strands at the grout/void interface. Visual inspection showed that a thin water pool existed there as late as 4 days after the event, possibly contributing to the observed corrosion of those strands. It should be noted however that the pH of recharge water (whether fresh or salty) temporarily remaining on top of the grout after wetting events was ~13. The strand-anchorage body conductance evolution in the P assemblies is shown in Figure 10. Each water recharge event was accompanied by an increase in conductance which dissipated after some time, roughly paralleling the length of time recharge water remained visible on the grout surface (Table 3).

Figure 11 shows the galvanic current trends in the S series assemblies. Unlike in the P assemblies, fresh water in the S assemblies triggered strong macrocell action (in agreement with the visual observations), and the strands behaved consistently as net anodes. This difference is partly explained by the greater chloride content in the S grout (500 ppm, Table 1) compared that in the P grout (80 ppm). Despite the relatively high native chloride content, recharge water was still needed to support corrosion at the grout/void interface, as evidenced by the rust free condition of that zone in Assembly S2 which was kept without external water contamination. On the other hand, even a small amount of fresh water (e.g. 10 ml in S3 at day 209) was enough to support significant strand corrosion. Conductance trends in the S assemblies (Figure 12) resembled those in the P assemblies, but with typical conductance values about one order of magnitude lower.

Figures 13 and 14 show representative potential trends of the interconnected strands-anchor system, using assemblies P2 and S1 as examples. Comparable trends were observed in the replicate assemblies. The potential trends correlate well with those of the galvanic

currents and suggest the presence of activation-passivation cycles linked to each recharge event. Spatial resolution is provided by measurements at ports at the various levels (Figure 3). Figure 13 shows that the first fresh water addition to P2 caused no large change on potentials (all remaining at ~-200 mV vs SCE) at either the top, middle, and bottom locations. This is indicative of passive behavior at all levels, unaffected by the fresh water addition, and in agreement with the macrocell current behavior noted above. However, recharge with the salty solution caused instantaneous excursions to much more negative potentials, indicative of depassivation and consistent with the macrocell current increase. The potential excursions at the upper levels (by the grout-void interface) were larger, in agreement with the externally observed corrosion location. Comparable trends are seen in Figure 14 for assembly S1. However, in this case the potentials at the top and grout surface locations gradually increased to above -200 mV as repassivation followed a recharge event, but the potential readings at the middle and bottom locations did not completely recover to about -200 mV before next water recharge event. This suggests that some corrosion might extend to regions far below the main grout/void interface.

Grout Properties and Steel Polarization

Bleed Water. Only a very small (~<0.1%) amount of bleed water was seen around the strand area for the commercial grouts A~D and only about 0.3% bleed for grout E. In contrast, there was ~1.6% bleed water for the plain paste specimens.

Grout Resistivity: As shown in Figure 15, the change of resistivity with time (results of multiple specimens of each type) follows some common trends. All the newly-cast grouts, although with different water to grout ratios (W/G), had a similar initial low resistivity value (~100 Ohm-cm) during the first 10 hours, followed by a sharp increase to ~1000 Ohm-cm during the next 20 hours. All the grout resistivities kept increasing next, reflecting the continuing hydration process with corresponding self-desiccation and reduced connectivity of the pore network. Later on the resistivity of the commercial grouts began to approach apparent terminal values ranging from ~8 KOhm-cm to ~50 KOhm-cm The apparent terminal resistivity of the plain cement pastes, with a water to cement ratio (W/C) of 0.45, was much lower than that of the commercial grouts (W/G 0.23 to 0.30). Based on these findings and the evidence for self-dessication in the next item, grout resistivity values from 10^3 to 10^5 Ohm-cm were used as ranging input parameters in the modeling calculations presented later.

Internal RH. The results (Figure 16) show decreasing trends with time but with distinctly higher apparent terminal values (>90%) for the plain paste grout with or without expansive agent addition, than for the commercial grouts. These show long term trends toward values <80%, reflecting significant self-dessication [Bentz, 2001] as might be expected from the small water content used. The decreasing RH trends correlate well with the increasing resistivity trends shown above.

Pore water pH. All the grouts in a mature condition and isolated from external air, showed (Figure 17) high pore water pH values in the range (~13.2 to ~13.7). That range was comparable with values commonly observed in regular concrete and mortar applications [Sagüés, 1998]. These values are also consistent with the observation of pH=13 for the surface water of the mock-up assemblies shortly after placement of the recharge water.

Carbonation. The result of exploratory carbonation measurements are shown in Table 4. The carbonation penetration was too small for detection in grouts B and C, but those findings would need further examination to rule out possible evaluation artifacts. The carbonation coefficients of the other commercial grouts were comparable to those encountered in atmospherically exposed moderate to low quality concrete [Alonso, 1993], while in the plain cement grouts the coefficients were even greater. These high carbonation penetration rates are consistent with the relatively high porosity (next item) of the grouts and, in the case of the commercial grouts, the tendency to self-desiccation noted above.

Porosity. Volumetric porosity (Figure 18) of commercial grouts (average of multiple specimens of each) ranged from ~25% to ~35%. Porosity of the plain cement grout was ~45% and ~37% without and without expansion agent respectively. These high values are consistent with common observations of grout behavior and with the trends recorded elsewhere in this section.

Chloride Content.. Figure 19 shows chloride content (as ppm of dry material weight) of the as-received grout or cement stock, and the hardened grout as obtained from the top 2mm layer, the middle, or the bottom portion of the hardened 30 cm tall cylinder resulting from a bleed-water. In all cases the chloride content of the base stock was below the current FDOT specifications (800 ppm) acceptance level. The results do not show, for the conditions used in the bleed water test (top sealed from external environment) evidence of consistent strong accumulation at the top of the column. Figure 20 also shows results of analysis of dry stock and of powder samples obtained by scratching from the top grout surface of the P and S mock-up assemblies (PN and A materials respectively). Chloride content in the assembly grouts and base stock differed from that in the bleed tests, which may be ascribed to batch-to-batch variability. Even though higher than that for the bleed test, chloride content of stock in the S assembly was nevertheless below the specified limit. Since deionized water was used for mixing, the chloride content obtained reflects almost exclusively that originating from the initial cement or grout stock.

Steel Polarization: Figure 20 shows an example of oxygen reduction characteristics on duplicate PT wires at two immersion times in SCS. Similar cathodic polarization curves were obtained at 1 and 2 months, indicating a steady state had been reached. From these curves, an idealized Tafel slope value of 100 mV/decade was abstracted, together with a nominal exchange current density of 10^{-5} $\mu A/cm^2$ at a nominal equilibrium potential of 160 mV (SCE). The corresponding cathodic polarization line approaches the average trend (away from the open circuit potential) of the curves in Figure 20. Comparable results were obtained for SCS, SPS and the hardened grout, indicating relatively small variation of cathodic efficiency within the pH range present. The polarization behavior observed is also comparable to that seen for plain steel in similar environments [Li, 2001].

DISCUSSION

The following addresses the mechanism of depassivation, the location of corrosion, macrocell development, and the extent and timing of corrosion. Unless otherwise indicated, the discussion focuses in the scenario where much of the bleed water is reabsorbed into the grout

or evaporated away from the anchorages early in the life of the structure, and either terminal moisture regimes or episodic water recharge events are predominant.

Steel/Iron Depassivation in Mock-up Assemblies

In the grout: In the absence of recharge water both types of grout provided an environment conducive to passivation, at the grout-embedded zone, of both the strand steel and anchor ductile iron. Carbonation of the grout at the grout/void interface (from contact with the external air through the always-open port on the side) did not appear to have progressed to a large enough extent to spontaneously depassivate either material. Fresh recharge water in the low-chloride (80 ppm) P grout did not cause depassivation, but 0.01 N NaCl recharge water did for both strand and anchorage. For the higher chloride content (~500 ppm) S grout depassivation occurred with just fresh water addition. The eventual return to potentials commonly indicative of passive conditions [Glass, 1997] after long term drying is often observed in cementitious systems, and may partly reflect enrichment of the increasingly small amount of pore water with metal ions leading to formation of protective precipitates, overcoming the opposite tendency for sustained depassivation by local acidification.

The response to recharge events may be considered in the light of Figure 21, which summarizes results [Li, 2001; Hausmann, 1967] on the chloride content needed to initiate corrosion of plain steel in model solutions as function of solution pH. Values of pH expected for the pore solution of a typical grout not carbonated (in the order of those in Figure 17) and in a fully carbonated condition [Andrade, 1986] are shown as well. For a given hydrated grout saturated with external fresh water, the chloride content of the pore water depends on factors that include the native chloride content and the porosity ε of the hydrated grout, and the chloride binding isotherm of the system [Li, 2001]. Those factors can vary greatly, but for discussion representative values of ε=0.2, concrete density 2 g/cm^3, and roughly linear binding (on account of the low native chloride levels considered here) with a bound/free chloride ratio of 10:1 [Li, 2001] may be assumed. In such case the 80 ppm and 500 ppm native chloride levels would correspond to pore water concentrations in the order of ~0.0015 N and ~0.01 N respectively. Thus, a pore water pH of ~13 (as observed in the surface water) would still suffice to retain passivity in either case. However, if at some spots the pH were to fall by just ~1/2 unit (e.g. by localized carbonation) or if modest chloride evaporative concentration would occur, corrosion initiation could easily take place in the 500 ppm case. Conditions would have to be proportionally more severe to initiate corrosion by fresh water contact in the 80 ppm case (similarly assessments can be made for the chloride contents of the various other grouts addressed in Figure 19). These scenarios are consistent with the observation of corrosion upon fresh water addition in the S but not in the P grout, as well as the onset of corrosion in the P grout upon addition of 0.01 N NaCl recharge water. It may be concluded that conditions are dangerously close to steel depassivation in voided anchorages if openings to the exterior allow for even modest carbonation of the grout and periodic intrusion of even fresh water, if sufficient native chloride is present in the grout[A]. The responsible native chloride does not need to be very high, since 500 ppm in the hydrated grout corresponds to only ~600 ppm (0.06%) in the initial bagged product. Such content is below common current product specifications [0.08% per FDOT Specification 938] which may merit revision to lower levels in view of these findings. Control of chloride in the mixing water is equally critical.

[A] Carbonation-assisted corrosion initiation could be further promoted as time progresses if the interface were to become drier and a carbonation front penetrated faster into the grout.

In the air space: A thin layer of hydrated grout on the metal surface, left after bleed water receded, is not expected to be highly protective since it would become rapidly carbonated upon intrusion of external air. Depassivation in the air space would then be expected to develop relatively early, and the subsequent extent of corrosion would then be determined by the RH in the air space as discussed below. Where the residual grout is thicker, depassivation and subsequent corrosion may be determined by the degree of contact with water leaking in. In the assemblies examined here, conditions at thick grout residues just above the air-grout interface were relatively benign but it is not certain how general that situation may be.

Corrosion location

Grout/void interface: The findings confirmed the vulnerability of the system to corrosion at the grout-void interface, where depassivation is likely as indicated above. Whether corrosion in that region favors the strands or the anchorage depends in part on the nature of the mutual galvanic interaction, but it is of concern that the structurally critical strands were attacked in all three of the S assemblies and at least one of the P assemblies.

Inter-strand and grout-anchor gaps: Recharge fresh water trapped in inter-strand gaps (observed only in the S assemblies) appeared to have extended corrosion of the strands to those gap locations, as suggested by the potential differences between top and middle/bottom port readings noted above (Figure 14). This would not be surprising, as these interstices were likely efficiently exposed to external air during dry periods and the depassivation mechanism considered above for the main grout/void interface would apply equally. Corrosion of the anchorage at grout-anchor interstices would be suggested as well by the same potential observations and mechanism.

Air Space Corrosion: Severe corrosion of this type was observed primarily in the P series assemblies, on the interior surface of anchor and on the strands. The rust from air space corrosion was not uniformly distributed on the anchor but nevertheless covered about half of exposed surface area. Rust distribution on the strands varied greatly among the three assemblies depending on the amount of grout residue on the strands bundles left by bleed water. The incidence of air space corrosion in the P assemblies seems to be a direct consequence of the high internal RH of this material (~90%) noted earlier, which often resulted in condensation visible on the glass bell despite some contact with the external air. The observation of corrosion under these conditions is consistent with the sharp increase in corrosion rate when RH exceeds about 75% to 80% noted in studies of atmospheric corrosion of metals [ASM International, 1987]. In contrast, the S grout (terminal internal RH ~ 75%) showed fewer indications of severe air space corrosion. A similar beneficial effect may be expected from the other commercial grouts with low terminal RH (Figure 16).

Macrocell Development

The experiments showed substantial macrocell currents (e.g. 400 μA) developing between strand and anchorage in both types of grouts during simulated recharge events. The current persisted at lower levels (10 μA) for extended periods even in those cases where surface water was no longer present, indicating that the hydrated grout itself has significant conductivity to support galvanic action. The galvanic effect was always adverse to the strand (it became the net anode) in the S grout and in one of the recharge events in the P grout. These findings confirm similar effects observed in preliminary experiments [Powers 2002]. Moreover,

numerical simulation detailed later in the modeling section showed that under typical tendon conditions macrocell current between the active and passive regions on the strands could sustain a highly increased corrosion rate at an active area in the grout-void interface, even in the presence of only a moderate oxygen supply.

Extent/Timing of Corrosion

The presence of a bleed water void in a grouted system implies that the void was initially filled with bleed water that was subsequently reabsorbed and/or evaporated. While the void still contains a sizable amount of bleed water, significant corrosion could take place at the air-water interface by the mechanisms mentioned in the Introduction and assuming that oxygen availability were enough to support the necessary overall corrosion rate. Such evidence of corrosion activity was observed in the P mock-up test assemblies during the relatively brief initial period of free bleed water and in earlier work [Powers 2002]. A recent investigation by Bricker and Schokker found severe pitting of strand steel after sustained exposure to free bleed water for 6 months [Bricker 2005].

The present results indicate that in addition to early deterioration from free bleed water presence, much of the PT corrosion in grout voids during the life of a bridge may result from later recharge events associated with rainfall or condensation. The macrocell and potential measurements indicated that corrosion at the grout-void interface may be sustained for a long time (e.g. months) after a recharge event. Furthermore depending on the type of grout and extent of exchange with the outside environment, air space corrosion could conceivably proceed much longer after a recharge event.

In the following a rough durability estimate is made for the long term conditions indicated above. The mock-up test assemblies have been preserved for continuing exposure and direct measurements of corrosion damage are not yet available[B]. At present however, a working assumption was made that the total strand corrosion current is in the order of the anodic galvanic current measured. This assumption is not necessarily conservative, as local cell action is ignored, but both the findings from the Modeling section as well as prior experiments [Powers, 2002] suggest that it may be sufficient to obtain a rough indication of the expected damage. Since the grout-void interface corrosion appeared to be limited to a small zone, it was further assumed that the corroded zone affected a 1 mm high band around the strand bundle perimeter (surface ~2.5 cm^2). This approximation is also consistent with some of the scenarios addressed in the Modeling section. The metal loss was considered to affect equally each of the six strands in the perimeter, and the loss of any given strand was calculated as a simple percentage of its total 7-wire cross sectional area (~1.4 cm^2); detailed distribution among wires was not addressed. The results of this analysis are given in Figure 22 using the S assemblies as an example. The calculations project between ~0.4% and ~12% strand cross section loss after a period of 9 months with a few recharge events. These results are in the order of direct corrosion measurements obtained in a preliminary study using a mock-up assembly comparable to those used here [Powers, 2002]. There corrosion was in the form of pits, located in a region about 1-2 cm around the grout-air void interface. Maximum pit

[B] Corrosion rate measurements using polarization methods were performed separately and will be reported elsewhere.

depths ranged from 0.12 mm to 0.35 mm, so penetration depth was as much as ~7% of a wire diameter after only ~1/2 year of exposure.

A rough indication of the time required for outright overload failure of PT wires could be made based on common construction practice by conservatively assuming that the terminal stress in post-tensioned strands is on the order of 70% of the ultimate tensile strength. Thus, the occurrence of the failure of strands is likely to take place before corrosion from one side reduces the local cross section by ~30%. As a normally stressed strand could easily fail after 30% cross section loss by pit-like corrosion [Powers, 2002], fracture could take place after as little as a few years under these condition. Such projection, albeit based only on rough assumptions, is consistent with previous work [Powers, 2002] and with the observation of tendon failures in the field as early as after 7 years of service [Corven, 2001].

As a consequence, once corrosion attack initiated, the first wire failure under the average corrosion rates in the above examples could take place between < 1 year and ~ 30 years depending on oxygen availability. If corrosion were to be further localized as suggested by the results presented in the Modeling section, or due to the development of small pits, failure could occur even earlier in some instances. Any damage that took place while substantial bleed water was present earlier on would correspondingly shorten the time to failure.

Air space corrosion in the mockup anchorages has not been quantified yet, but preliminary examination of PT wires placed in a 100% humidity chamber showed pits with a maximum depth ~0.2mm after one year. If penetration depth progressed linearly and ~30% reduction of area could cause failure, then individual strand breaks could happen under sustained high humidity conditions after as little as ~3.5 years. Actual service conditions for this mode of corrosion may not be as severe if terminal RH is low, or if pitting progresses less than linearly with time, and additional work is in progress to better assess the potential extent and effects of air space corrosion.

MODELING

System Modeled

The objective of this section is to supplement the understanding of experimental findings provided above by means of an initial basic model that evaluates the contribution of individual factors to the overall observed corrosion. The system simulated was a simple grouted cylinder with an axially placed 19-strand bundle and a grout void at the top (see Figure 23). The complicating geometry issue of strand distribution in the polyethylene duct as in Figure 23(c) was not taken into consideration. It was simply assumed that only the outer surface of the strands bundle in Figure 23c) was electrochemically significant. Thus, an effective diameter of this equivalent was calculated from the total nominal cross section area of 19 0.6″-post-tensioning strands. A small 2 cm-long[C] segment on the top (corresponding to the region close to the anchorage plate and most likely affected by chloride contamination and

[C] It is noted that the model allows for non-uniform corrosion within the active zone, so the actual region of high corrosion rates can be significantly narrower than the 2 cm band of active material.

decreased pH) was designated as the actively corroding portion, while the rest of the surface area of the strands was treated as passive with only the cathodic reaction taking place on it.

In the present calculations galvanic coupling was limited to that existing between the active zone and the rest of the strand assembly. Coupling to the surrounding anchorage metal, which would increase the extent of macrocell currents, was not included in the present simulation but can be addressed in the future by straightforward expansion of the same basic model. However, as it will be shown the effect of a greater extent of galvanic coupling may be gleaned from the effect of changing other model parameters that increase electrochemical coupling between anodic and cathodic regions. Other factors such as effects from strand spreading (as opposed to being in a tight bundle) and non-uniform grout properties can likewise be addressed in subsequent modeling approaches.

Electrochemical reactions

In keeping with alkaline conditions, the only important cathodic reaction considered here was oxygen reduction (Eq.1). The only anodic reaction at the active segment of the strand was iron dissolution that was subject only to activation polarization (Eq. 2).

$$O_2 + 2H_2O + 4e \rightarrow 4OH^- \quad (1)$$

$$Fe \rightarrow Fe^{2+} + 2e^- \quad (2)$$

An additional anodic reaction, passive dissolution, was assumed to take place at the passive steel surface at a rate ip independent of potential. The cathodic reaction was assumed to take place at every point of the strand surface, at a rate given by the Bulter-Volmer equation (with concentration-dependence) as follows.

$$i_c = i_{oc} \frac{C}{C_0} e^{(\phi_s - E_{oc})/\beta_c} \quad (3)$$

The anodic reaction at the active steel surface was described by:

$$i_a = i_{oa} e^{(E_{oa} - \phi_s)/\beta_a} \quad (4)$$

The subscripts, c and a, denote cathodic or anodic reaction respectively (also see Nomenclature). These equations were put together in terms of local current densities, with exchange current density i_0, Tafel slope β, and nominal equilibrium potential E_0. ϕ_s is the potential at a point in the electrolyte adjacent to the strand surface. The strand itself was considered as an equipotential surface because of its high conductivity. The sign convention of the potential values was consistent with those published in previous papers [Kranc, 1994, 1997, & 2001].

Governing Equations: For simplicity, the grout used in the system was treated here as a homogeneous medium, which had constant electrical conductivity, σ, and oxygen diffusivity, D. Therefore, the governing equations at steady state for the electrical potential and oxygen diffusion in the grout could be expressed as Laplace's equation:

$$\nabla^2 \phi = 0 \tag{5}$$

$$\nabla^2 C = 0 \tag{6}$$

Boundary conditions

Per Ohm's law, the normal gradient (radial *r* direction) of the potential in the grout at the strand surface is proportional to the sum of all the current densities, that is, the net current across the electrolyte must match the net rate of electrochemical reactions. For oxygen transport at the strand surface, the local net O_2 supply, formulated by Fick's first law, was made to match the amount consumed by the cathodic reaction. The boundary conditions at longitudinal z direction and radial r direction are listed below. A detailed explanation of this approach is given elsewhere [Kranc, 1997 & 2001].

$$\sigma \frac{\partial \phi}{\partial r} = \sum i = i_a + i_c \quad \text{(active surface)} \tag{7}$$

$$\sigma \frac{\partial \phi}{\partial r} = \sum i = i_c + i_p \quad \text{(passive surface)} \tag{8}$$

$$\frac{\partial C}{\partial r} = \frac{i_c}{4DF} \quad \text{(active and passive surface)} \tag{9}$$

Dimensionless Equations

The above governing equations and boundary conditions can be cast in dimensionless form with the following definitions:

Variables: $Z' = \frac{Z}{L}$, $r' = \frac{r}{R}$, $C' = \frac{C}{C_0}$, $\phi' = \frac{\phi - E_{corr}}{\beta_a}$

Input parameters: $K = \frac{L}{R}$, $\xi = \frac{4FDC_0}{Ri_{corr}}$, $\eta = \frac{\sigma \beta_a}{Ri_{corr}}$ (Wagner Number), $i_p' = \frac{i_p R}{\sigma \beta_a}$

$$\beta_a' = \frac{\beta_a}{\beta_a} = 1, \quad \beta_c' = \frac{\beta_a}{\beta_c}$$

Substitution of these definitions into the governing equations yields:

$$\frac{\partial^2 \phi'}{\partial Z'^2} + K^2 \frac{\partial^2 \phi'}{\partial r'^2} + K^2 \frac{1}{r'} \frac{\partial \phi'}{\partial r'} = 0 \tag{5′}$$

$$\frac{\partial^2 C'}{\partial Z'^2} + K^2 \frac{\partial^2 C'}{\partial r'^2} + K^2 \frac{1}{r'} \frac{\partial C'}{\partial r'} = 0 \tag{6′}$$

In terms of dimensionless variables, the boundary conditions on the steel surface become

$$\frac{d\phi'}{dr'} = \frac{1}{\eta} C' 10^{(\beta_c' \phi')} - i_p' \tag{7′}$$

$$\frac{d\phi'}{dr'} = \frac{1}{\eta} C' 10^{(\beta_c' \phi')} - \frac{1}{\eta} 10^{(\beta_a' \phi')} \tag{8′}$$

$$\frac{dC'}{dr'} = \frac{1}{\xi} C' 10^{(\beta_c' \phi')} \qquad (9')$$

In the calculation, a finite difference formulation on a matrix of 201 nodes on the axial direction and 16 nodes on the radial direction was used and non-uniform grid size was adopted to simulate a 3 m-long system. Typically over 5×10^5 iterations were conducted to approach convergence, which was evaluated by observing the difference between the total computed anodic and cathodic current of the system. The final difference between those currents was typically less than 2%.

Cases Modeled

Two cases based on oxygen availability at steel surface were modeled as outlined below. In both cases the air void is conservatively assumed to be in sufficient contact with the external air (through inefficient sealing of the anchorage wedge plate area) to maintain a near-atmospheric oxygen content.

Case A series. Limited grout oxygen transport was assumed, that is, oxygen could only diffuse through the grout surface in contact with the air void and (to a much lesser extent) the lateral surface in contact with the HDPE duct. This assumption simulated an ideal condition, in which there were no cracks on the plastic duct. Additionally, the interstices between the king wire (central wire of an individual strand) and surrounding wires or inner strands and outer strands or any other deficiencies were assumed to be blocked and hence oxygen could not diffuse through this pathway either. The oxygen concentration (expressed in terms of the concentration of oxygen present in the grout pore solution) at the void air-grout and external air-duct interfaces was chosen as a constant 3×10^{-7} moles/cm^3 [Kranc, 2001], which is representative of equilibrium with the atmosphere as it may happen at the anchorage if sealing is not complete. All diffusivity values were converted to correspond to the manner in which oxygen concentration was expressed. Based on the oxygen diffusivity and solubility values in HDPE per literature references [Rharbi, 1999, Epacher, 2000], the diffusion coefficient of oxygen there, D_{HDPE}, was set as 10^{-7} cm^2/s which is 1/100 of a typical value of oxygen diffusivity in water (10^{-5} cm^2/s). Other parameters used in the calculations are listed in Table 5 The grout conductivity (resistivity) value range examined brackets the values obtained for the plain cement and commercial grouts presented in the experimental results section. Grout oxygen diffusivity values examined also bracket plausible values for cementitious materials in various stages of curing or drying. [Tuutti 1982]. Reliable experimental anodic parameters for post-tensioning wires are not available at present, so for the purpose of these calculations values were chosen to be representative of the range commonly assumed for steel in concrete [Naish, 1990, Kranc, 1997].

Case B series. An oxygen concentration representative of atmospheric equilibrium (3×10^{-7} moles/cm^3) was available at all locations throughout the grout. This presented the worst condition (severe HDPE duct splitting and essentially free air transport through the interstices among strands, or through anchor-grout gaps as those noted in the experimental results section) for corrosion attack since cathodic reduction of oxygen was not concentration dependent anymore.

Modeling Results and Interpretation

Figure 24 illustrates the resulting oxygen concentration along the strand surface for the 10^4 Ohm-cm resistivity calculations. Oxygen concentration drops greatly in the active region due to the high consumption of oxygen associated with high local corrosion rate. At points far enough away from the active region, the oxygen demand decreases dramatically and the small flux through the HDPE duct wall (or alternatively through any minor leaks) is sufficient to finally maintain the surface concentration close to the atmospheric value. As expected, the oxygen concentration at the steel surface at or near steel surface becomes much lower for the lower grout oxygen diffusivity values. As seen in Figure 25, the active and passive regions are distinctly separated due to the model assumptions which cause those regions to behave as a net anode and a net cathode respectively. Two opposite factors influence the anodic current density profile in the first 2 cm (the active region): 1) decreasing oxygen concentration in the case A series and 2) increased coupling between the active and passive region as distance from the origin increases. Therefore, for the case A series where diffusivity is finite, the magnitude of the anodic current density in the active region first decreases with depth and then increases closer to passive steel zone. It is noted that for medium to low oxygen diffusivity conditions the corrosion rates are high at the air space-grout interface but drop sharply with depth into the grout. This condition suggests localization of corrosion near the surface and is in keeping with the assumption of a narrow corrosion band (e.g. 1 mm) for the approximate durability estimate made in the discussion of the experimental results that addressed relatively wet (and consequently low oxygen diffusivity [Tuutti 1982]) conditions. For the case B series with unrestricted oxygen access, the anodic current density does not experience an initial decrease. These trends are reasonably as expected and suggest that the model, despite its simplicity, may provide useful insight for understanding the otherwise complex conditions in an actual grouted anchorage system.

Figure 26 shows how the computed average corrosion current density over the total active region surface area depends on grout resistivity and oxygen diffusivity. Under the present assumptions, the calculations indicated that oxygen access as a dominant factor and the results were least sensitive to grout resistivity. For any given diffusivity, varying resistivity over two orders of magnitude changed the current density by less than one order of magnitude (although at very high resistivity the availability of electrolyte could be a limiting factor not included in the present model assumptions). In contrast, for example at a resistivity value of 10^4 Ohm-cm, the average corrosion current density increased from 4 to 73 $\mu A/cm^2$ when increasing oxygen diffusivity from 10^{-5} to 10^{-3} cm^2/s. Unrestricted oxygen access yielded 159 $\mu A/cm^2$. The above is a relative sensitivity comparison and does not imply that the contribution of resistivity (and consequently of macrocell coupling) to corrosion damage is negligible. Indeed Figure 25 implies that for moderate to low oxygen transport scenarios macrocell coupling represents a significant fraction of the corrosion current. The effect is expected to be appreciable larger if the model were to be extended to include the larger additional cathodic surface provided by the surrounding anchorage body. Thus, equating macrocell and corrosion currents for durability estimates (as done in the discussion of the experimental results) appears to be justified for simplified order-of-magnitude projections in the absence of direct corrosion rate evaluations. The corresponding average corrosion rates (by Faradaic conversion assuming formation of Fe^{++} ions) ranged from ~0.05 mm/y to ~2 mm/y and are roughly consistent with the estimates detailed in the experimental aection, as well as observations in preliminary experimental work [Powers 2002].

The overall modeling results are generally in keeping with expected behavior and the experimental observations. As indicated above, further modeling development should address other critical issues, notably galvanic coupling, the effect of periodic water recharge (involving the electrolyte availability issue mentioned above), iron dissolution kinetics, and the geometric distribution of grout and strands need to be incorporated in the model as well. Finally, the calculated cathodic current densities in these initial computations tended to extrapolate beyond the range of available data (Figure 20) so additional polarization data spanning a wider potential range should be developed.

CONCLUSIONS

1. Beyond the initial free bleed water stages, conditions leading to strand steel depassivation can develop in anchorages with grout voids if openings to the exterior allow for even modest carbonation of the grout and periodic water intrusion.

2. Fresh water recharge could initiate corrosion if the native chloride content of the grout exceeds a relatively small amount (e.g. 600 ppm). Currently allowable chloride limits may need revision.

3. Galvanic coupling between strand steel and anchorage iron can significantly aggravate corrosion of the strands.

4. Corrosion of strands in the air void space can be considerable, especially in grouts that support a high internal RH.

5. Projections of the combined effects of the deterioration mechanisms identified here are consistent with the observation of tendon failures after as little as a few years of service.

6. Grouts meeting present qualification criteria had electric resistivity that increased with time toward apparent terminal values of about 10^4 Ohm-cm and higher, suggesting that significant self-desiccation was taking place.

7. Oxygen-reduction polarization parameters of high strength wires in alkaline solutions representing grout, and in hardened grout, depended weekly on pH and were comparable to those encountered on plain steel in similar environments.

8. A simplified mathematical model of a corroding strand bundle was formulated, incorporating both polarization and oxygen transport behavior. This initial computational study indicated that oxygen availability is a key factor in determining corrosion severity. Grout resistivity was a secondary but still important factor within the range of validity of the model assumptions. Predicted corrosion rates were in general agreement with field and laboratory observations. Issues for subsequent model development were identified.

NOMENCLATURE

ϕ potential at a point of the electrolyte (all the potentials are in the saturated calomel electrode SCE, but referred to the metal, which was assigned to Zero potential. Note that this convention is the reverse of that commonly used to represent experimental data.)
σ grout conductivity
ξ dimensionless group for oxygen reduction boundary condition
η dimensionless group (Wagner Number)
β_a activation Tafel constant for iron dissolution (mV/decade)
β_c activation Tafel constant for oxygen reaction (mV/decade)
C effective oxygen concentration at any point in the concrete (mole/cm^3) (For the calculations, C was expressed in terms of the concentration of oxygen present in the grout pore solution, which was assumed to be in equilibrium with any surrounding gas.)
C_0 effective oxygen concentration at grout surface
d thickness of HDPE wall
D effective diffusion coefficient of oxygen in grout
D_{HDPE} effective diffusion coefficient of oxygen in HDPE duct
E_{0c} equilibrium potential for the cathodic reaction of oxygen
E_{oa} equilibrium potential for the anodic reaction of iron
F Faraday's constant
i_a anodic current density for iron
i_{oa} exchange current density for the anodic reaction of iron
i_{oc} exchange current density for the cathodic reaction of oxygen on iron
ip passive current density of iron dissolution
r radial direction
R_0 radius of the high-density polyethylene duct
R_1 radius of the nominal strand
Z longitudinal direction

Superscript

′ dimensionless definitions

REFERENCES

Alonso, C. and Andrade, C. "Life Time of Rebars in Carbonated Concrete", 10th Eyropean Corrosion Congress, Barcelona, Spain, Paper No. 165 (1993).

Andrade, C. and Page, C. L.. "Pore Solution Chemistry and Corrosion in Hydrated Cement Systems Containing Chloride Salts: A Study of Cation Specific Effects" *Br. Corros. J*. 21(1), p49, (1986)

ASM International, Metals Handbook, Vol. 13, 9th. Ed., ASM, Metals Park, p.82, 1987.

Bentz, D.P., Hansen, K.H., and Geiker, M.R., “Shrinkage-Reducing Admixture and Early Age Desiccation in Cement Pastes and Mortars”, Cement and Concrete Research, 31(7), p1075, (2001).

Bricker, M. D. and Schokker, A. J., "Corrosion from Bleed Water in Grouted Post-Tensioned Tendons", Research and Development Bulletin RD137, ISBN 0-89312-239-4, Portland Cement Association, Skokie, 2005.

Castro, P., Sagüés, A.A., Moreno, E.I., “Characterization of Activated Titanium Solid Reference Electrodes for Corrosion Testing of Steel in Concrete”, Corrosion, 52(8), p609 (1996).

Corven, J., “Mid Bay Bridge Post-Tensioning Evaluation”, Final Report, Florida Department of Transportation, October, 2001 http://www.dot.state.fl.us/structures/posttensioning.htm

Enos, D.G., Williams, A.J., Scully, J.R., “Long-Term Effects of Cathodic Protection on Pre-stressed Concrete Structures: Hydrogen Embrittlement of Pre-stressing Steel,” Corrosion, 53, 11, p891 (1997)

Epacher, E., Tolveth, J., Krohnke, C., Pukanszky, B., “Processing Stability of High Density Polyethylene: Effect of Adsorbed and Dissolved Oxygen”, Polymer, 41, p8401 (2000).

FDOT (Florida Department Of Transportation), “Sunshine Skyway Bridge Post-Tensioned Tendons Investigation”, Feb, 2002 http://www.dot.state.fl.us/structures/posttensioning.htm

Fontana, M., "Corrosion Engineering", 3rd. Ed., McGraw-Hill, New York, 1985.

Ghorbanpoor, A., Madathanapalli, S.C., “Performance of Grouts for Post-Tensioned Bridge Structures”, Report NO. FHWA-RD-92-095, National Technical Information Service, Springfield, VA, 1993.

Glass, G. K. and Buenfeld, N. R.. “The Presentation of the Chloride Threshold Level for Corrosion of Steel in Concrete”, *Corrosion Science*, 39 (5), 1001-1013 (1997).

Harkins, P., “Product Evaluation and Qualified Products List J-Grout/Mortar” Florida Department of Transportation, Aug, 2002, http://www.dot.state.fl.us/specificationsoffice/

Hausmann, D.A., Materials Protection, 6(10), p19 (1967).

Jones, D., “Principles and Prevention of Corrosion,” 2nd ed., Prentice Hall, 1996.

Kranc, S.C., and Sagüés, A.A., “Computation of Reinforcing Steel Corrosion Distribution in Concrete Marine Bridge Substructures”, Corrosion, 50(1), ,p50 (1994).

Kranc, S.C., and Sagüés, A.A., “Detailed Modeling of Corrosion Macrocells on Steel Reinforcing in Concrete,” Corrosion Science, 43, p1355 (2001).

Kranc, S.C., and Sagüés, A.A., “Modeling the Time-Dependent to External Polarization of a Corrosion Macrocell on Steel in Concrete”, Journal of Electrochemical Society, 144(8), p2643 (1997).

Krumbach, R., Konig, G., “Hydrogen Induced Stress Corrosion of Pre-stressing Steels-Introducing A New Testing Method,” 2nd Int. PhD Symposium in Civil Engineering, Budapest 1998.

Li, L., Sagüés, A.A., “Chloride Corrosion Threshold of Reinforcing Steel in Alkaline Solutions-Open-Circuit Immersion Tests”, Corrosion, 57, p19 (2001).

Morris, W., Moreno, E.I., and Sagüés, A.A., “Practical Evaluation of Resistivity of Concrete in Test Cylinders Using a Wenner Array Probe”, Cement and Concrete Research, 26(12), p1779 (1996).

Moreno, E.I., Sagüés, A.A., “Carbonation-Induced Corrosion of Blended-Cement Concrete Mix Designs for Highway Structures”, Paper No. 636, Corrosion/98, NACE International, Houston, 1998.

Naish, C., Harker, A., and Carney, R., “Concrete Inspection: Interpretation of Potential and Resistivity Measurements”, In Corrosion of Reinforcement in Concrete, C. Page, K. Treadaway, and P. Bamforth, Eds., Elsevier Applied Science, London-New York, p314, 1990.

Powers, R.G., “Corrosion Evaluation of Post-tensioned Tendons on the Niles Channel Bridge”, Florida Department of Transportation, Gainesville, FL, June, 1999.

Powers, R.G., Sagüés, A.A., Virmani, Y.P., "Corrosion of Post-Tensioned Tendons In Florida Bridges", Proceedings, 17th. U.S.-Japan Bridge Engineering Workshop, Nov. 12-14, 2001, Public Works Research Institute, Japan, Technical Memorandum of PWRI No. 3843, Hiroshi Sato, Ed. pp. 579-594, PWRI, 2002.

Preston, H.K., “Handling Prestressed Concrete Strand,” PCI Journal, November, p68 (1990).

Proverbio, E., and Longo, P., “Failure Mechanisms of High Strength Steels in Bicarbonate Solutions Under Anodic Polarization,” Corrosion Science, 45, p2017 (2003).

Rharbi, V., Yekta, A., and Winnik, M.A., “A Method for Measuring Oxygen Diffusion and Oxygen Permeation in Polymer Films Based on Fluorescence Quenching”, Anal. Chem., 71,, p5045 (1999).

Sagüés, A.A., Moreno, E.I. and Andrade, C., "Evolution of pH During In-Situ Leaching in Small Concrete Cavities", Cement and Concrete Research, Vol. 27, p.1747 (1997).

Sagüés, A.A., Kranc, S.C., and Hoehne, R.H., “Initial Development of Methods for Assessing Condition of Post-Tensioned Tendons of Segmental Bridges”, May, 2000.
http://www.dot.state.fl.us/research-center/

Sagüés, A.A., Powers, Rodney, G., Wang, H.B., “Mechanism of Corrosion of Steel Strands in Post Tensioned Grouted Assemblies,” NACE2003, Paper No. 03312, Corrosion/2003, NACE International, Houston, 2003.

Tabatabai, H., Ciolko, A. T., and Dickson, T. J., “Implications of Test Results from Full-Scale Fatigue Tests of Stay Cables Composed of Seven-Wire Prestressing Strands,” Proceedings of the Fourth International Bridge Engineering Conference, Vol. 1, August 28-30,, p. 266, 1995.

Tuutti, K., "Corrosion of Steel in Concrete" (ISSN 0346-6906), Swedish Cement and Concrete Research Institute, Stockholm, 1982.

Toribio, J., Ovejero, E., “Microstructure Evolution in a Pearlitic Steel Subjected to Progressive Plastic Deformation,” Materials Science and Engineering, A234-236, p579 (1997).

Wang, H., Sagüés, A.A. and Powers, R.G., "Corrosion of the Strand-Anchorage System in Post-Tensioned Grouted Assemblies" Paper No. 05266, Corrosion/2005, NACE International, Houston, 2005.

Table 1 Properties of the Anchor-Strands-Grout Assemblies

	Non-commercial grout P series	Commercial grout S series
Number of assemblies	3	4
Grout type used in the assemblies	Plain cement paste (Type I) at 0.45 water to cement ratio with 1%w aluminum based expanding admixture	Commercial grout S from FDOT qualified product list, received from commercial supplier (0.21water to grout ratio)
Assembly designations	P1, P2, P3	S1, S2, S3, S4
Cast date	8/13/2003	12/5/2003
Number of strands	7	7
Vibration*	Yes	No
Expansion of grout	~5.0 cm in depth	No
Grout bleeding	~1.5 cm in depth	No
Date (#days from casting) anchor and strands were connected for galvanic coupling	2	0
Chloride Content in original grout powder	5 ppm	550 ppm
Total Chloride Content in hardened grout	~80 ppm	~500 ppm

Table 2 Chemical Analysis of Alloys

	C	Si	P	Cr	Ni	Mn	Cu	Mo	Fe
PT Strand	0.81	0.26	0.009	0.12	0.04	0.71	0.1	<0.01	Bal.
Cast-Iron	3.61	2.88	0.012	0.02	0.01	0.25	0.11	<0.005	Bal.

Table 3. Test Data and Events for Mock-up Assemblies

Recharge Events		Non-commercial grout P series			Commercial grout S series			
Assembly #		P1	P2	P3	S1	S2	S3	S4
Days bleed water present on top		10	5	2	No bleed water from start			
First	Addition day	Day 35*			Day 56			
	Amount and type of recharge water	100 mL fresh	100 mL fresh	100 mL fresh	100 mL fresh	NO	NO	100 mL fresh
	Days water was visible on top of the grout surface	162	78	6	<1	-	-	<1
Second	Addition day	Day 179			Day 133			
	Amount and type of recharge water	NO	100 mL 0.01N NaCl	100 mL 0.01N NaCl	100 mL fresh water	NO	100mL fresh water	100 mL fresh water
	Days water was visible on top of the grout surface	-	69	5	<1	-	1	<1
Third	Addition day	Day 245			Day 209			
	Amount and type of recharge water	NO	100 mL 0.01N NaCl	100 mL 0.01N NaCl	100 mL fresh	NO	10 mL fresh	100 mL fresh
	Days water was visible on top of the grout surface	-	70	2	9	-	<1	9
Fourth	Addition day	Day 321						
	Amount and type of recharge water	100 mL 0.01N NaCl	100 mL 0.01N NaCl	100 mL 0.01N NaCl				
	Days water was visible on top of the grout surface	1	>68	6				

Notes: *counting from the day grout was cast into assemblies

Table 4. Exploratory Carbonation Tests

Grout Type	W/G	Top			Bottom			Circumference		
		Penetration Type*	Carbonation Coefficient ($mm/y^{1/2}$)**		Penetration Type	Carbonation Coefficient ($mm/y^{1/2}$)**		Penetration Type*	Carbonation Coefficient ($mm/y^{1/2}$)**	
			Min.	Max.		Min.	Max.		Min.	Max.
A	0.23	Continuous	1.3	1.3	Continuous	1.3	1.3	Localized	---	2.7
A	0.25	Continuous	1.3	1.3	Continuous	1.3	1.3	Localized	---	1.3
B	0.29	---	---	---	---	---	---	---	---	---
C	0.28	---	---	---	---	---	---	---	---	---
D	0.32	Continuous	4.0	4.0	Localized	---	---	Localized	---	4.0
E	0.28	Continuous	1.3	6.7	Continuous	0.7	4	Continuous	1.3	8
E	0.30	Continuous	2.7	2.7	Continuous	1.3	2.6	Continuous	1.3	6.7
E	0.31	Continuous	2.7	2.7	Continuous	1.3	5.3	Continuous	1.3	6.7
PN	0.45	Continuous	22.5	22.5	Continuous	3.7	3.7	Continuous	4.6	4.6
P	0.45	---	---	---	Localized	---	6.7	Localized	---	9.3

*Continuous/Localized denotes penetration occurred along the entire perimeter examined or was limited to parts of it.
**Dashes indicate penetration was too small to be observed at the time of examination (138 days).

Table 5. Modeled System Dimensions and Calculation Parameters (see Nomenclature)

Parameter	Value	Parameter	Value
L (cm)	307.7	E_{oa} (mV vs SCE)	780
R_0 (cm)	5.08	E_{oc} (mV vs SCE)	-160
R_1 (cm)	3.32	ioa (A/cm2)	3×10^{-8}
C_0 (mol/cm^3)	3×10^{-7}	ioc (A/cm2)	1×10^{-11}
D (cm2/s)	0.001	βa (mV/decade)	60
σ $(\Omega\text{-cm})^{-1}$	0.00001~0.001	βc (mV/decade)	100
$\rho(\Omega\text{-cm})$ $(1/\sigma)$	1000~100000	ip (A/cm^2)	10^{-8}
d (cm)	0.25		

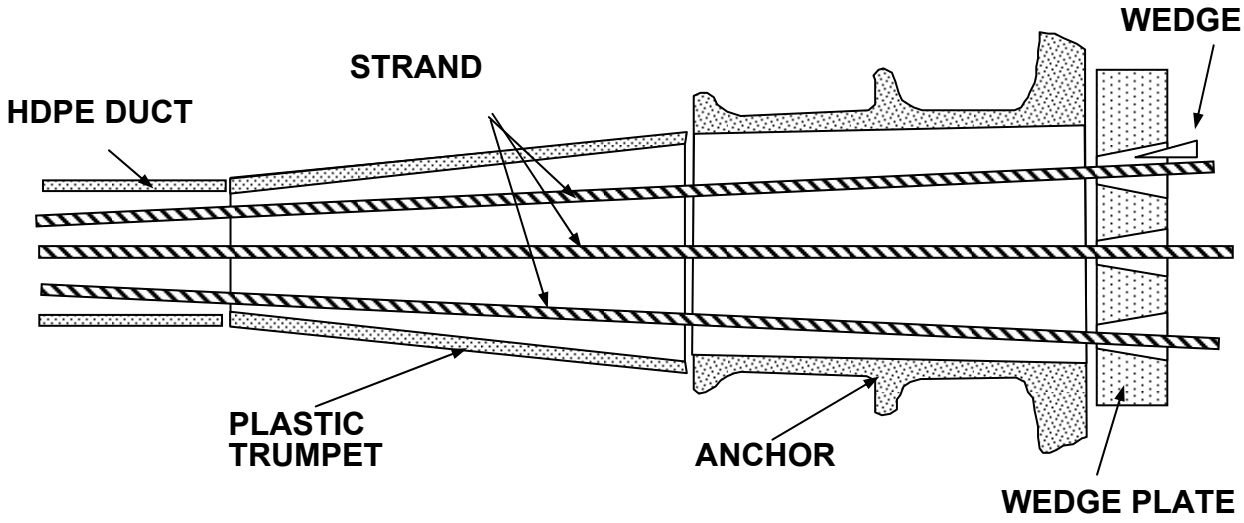

Figure 1. Idealized schematic of a typical anchorage system. Only 3 strands shown for clarity. Anchor, wedge plate and wedges are ferrous alloys

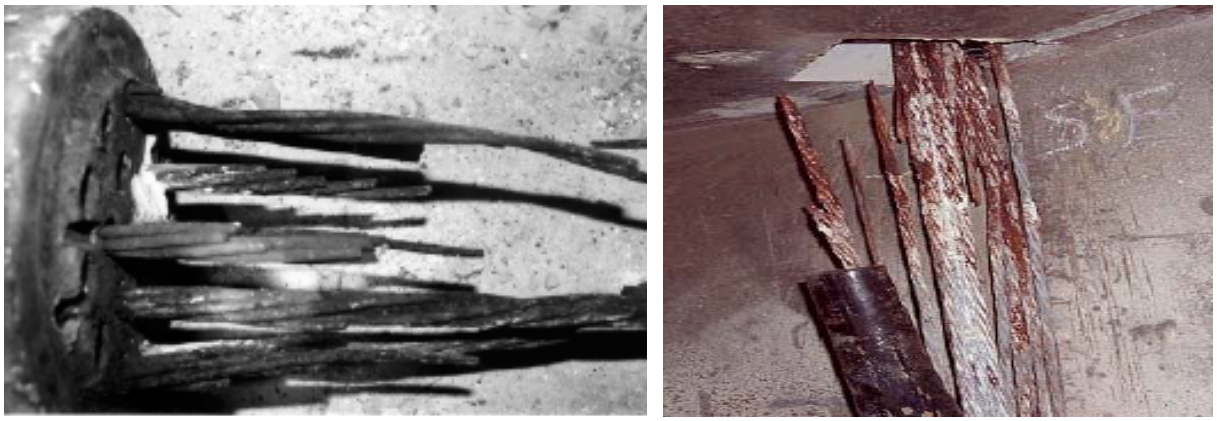

Figure 2. Severe failure of post-tensioning tendons near cap region
Left: Failed tendon at Niles Channel Bridge (Powers, 1999)
Right: Failed tendon at Column 133 NB of Sunshine Skyway Bridge (FDOT).

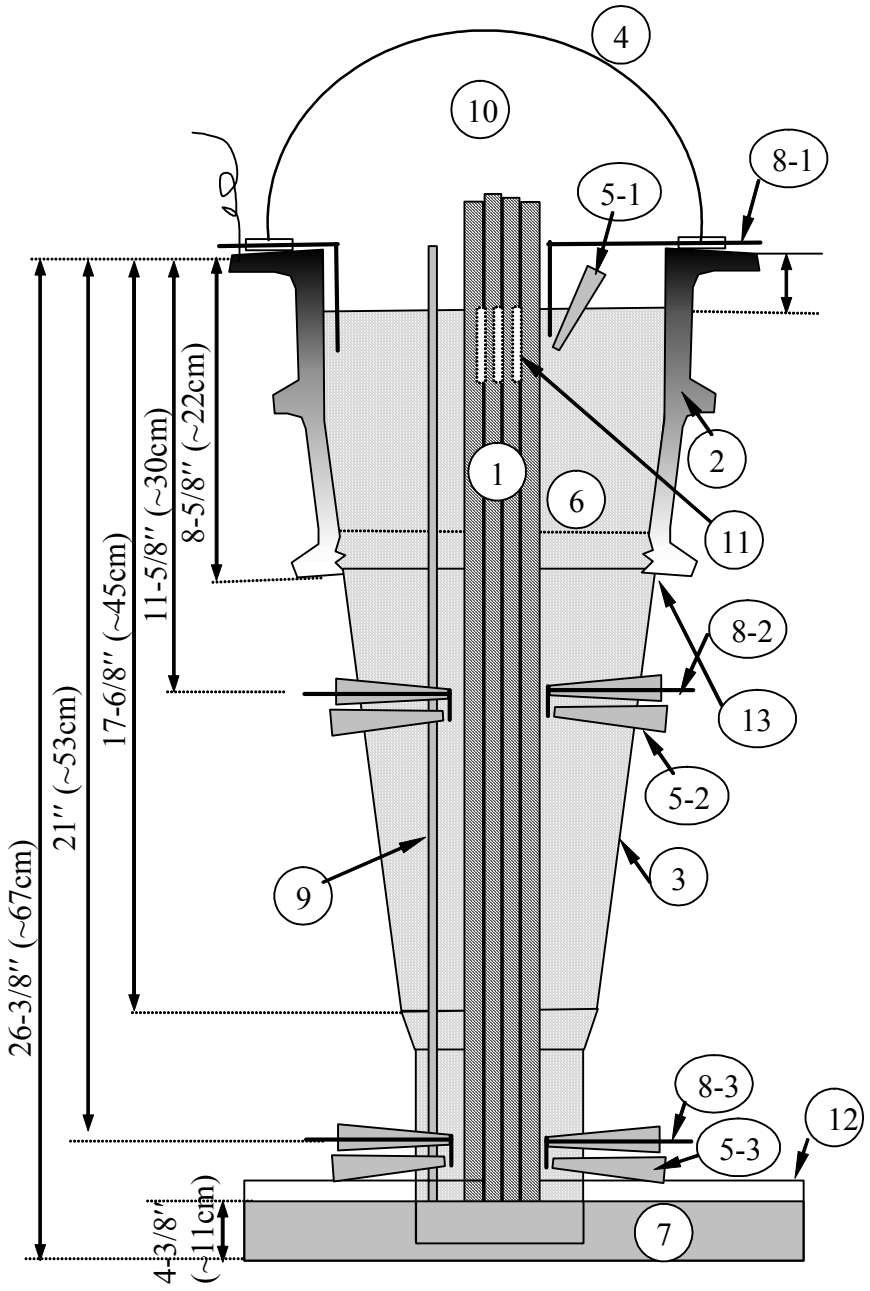

Figure 3a. Schematic of anchor test assembly.
1. 7 PT strands bundle; 2. Cast-iron anchor; 3. HDPE trumpet; 4. Glass cover; 5-1,2,3. Potential ports at top, middle, and bottom, respectively; 6. Grout; 7. Cement paste base; 8-1,2,3. Ti wire reference electrodes at top, middle, and bottom, respectively; 9. Ti Counter electrode; 10. Void; 11. Inter-strands void if present; 12. Plastic pan; 13. Plastic trumpet - anchor joint.

Figure 3b. Anchor test assemblies.

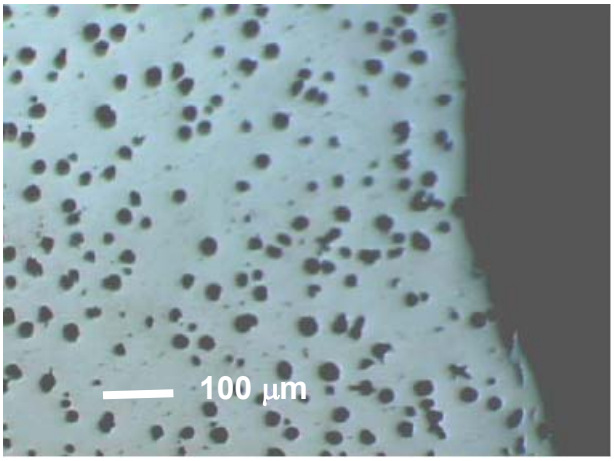

Figure 4. Micrograph of ductile cast-iron anchor body steel showing spheroidal graphite nodules.

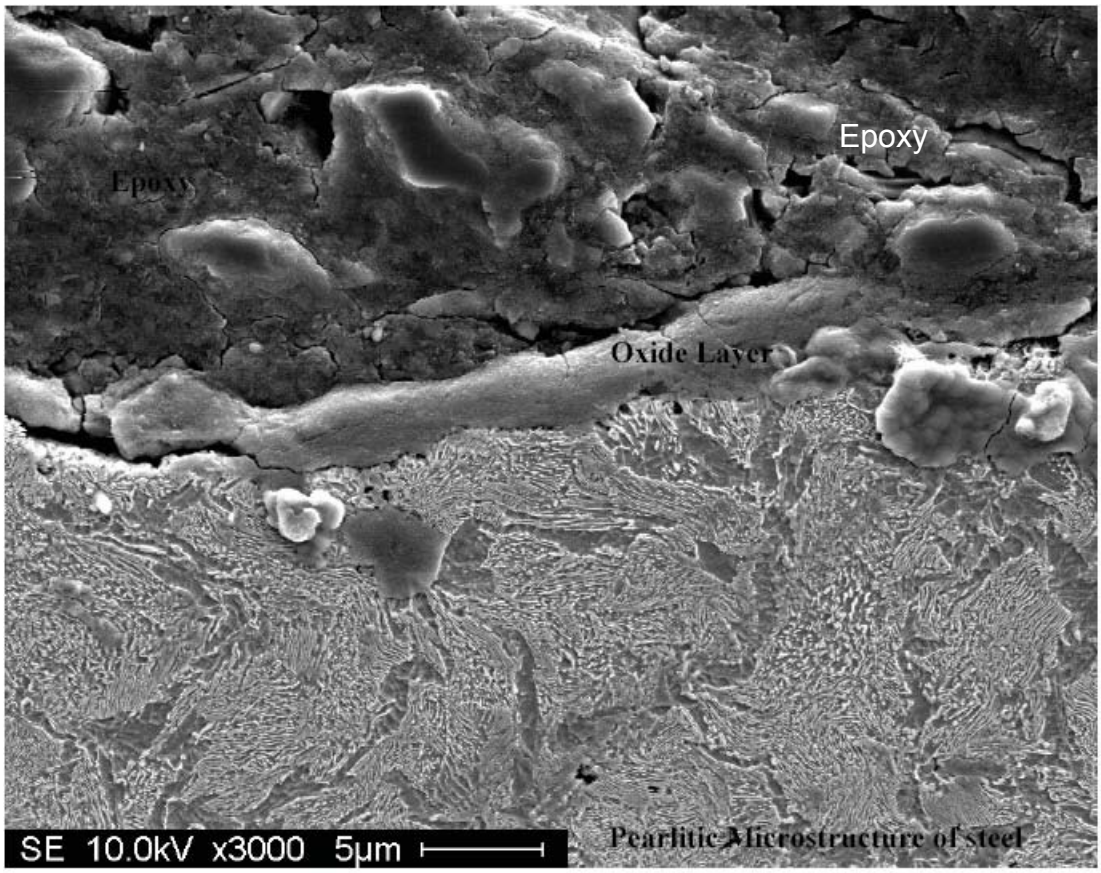

Figure 5 a. Microstructure of high-strength pt strand wire transverse section with thin oxide film

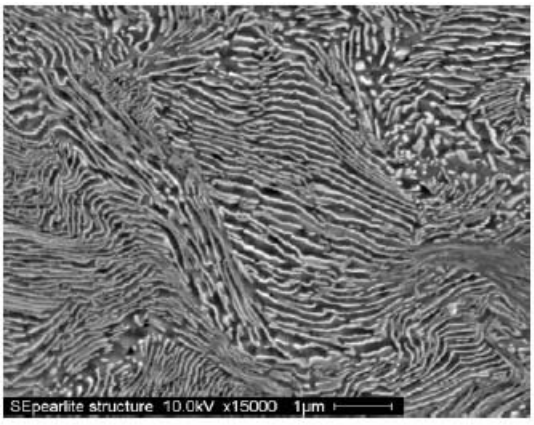

(b) Fine pearlitic microstructure in transverse section

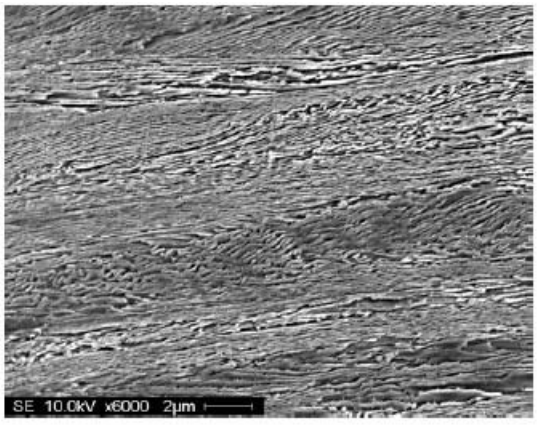

(c) Fine pearlitic lamellae parallel to the axis of wire due to cold drawing

Figure 5 b-c. Microstructure of high-Strength PT strand wire.

Figure 5d. ISL test specimens in 100% RH chamber for determination of pore water pH.

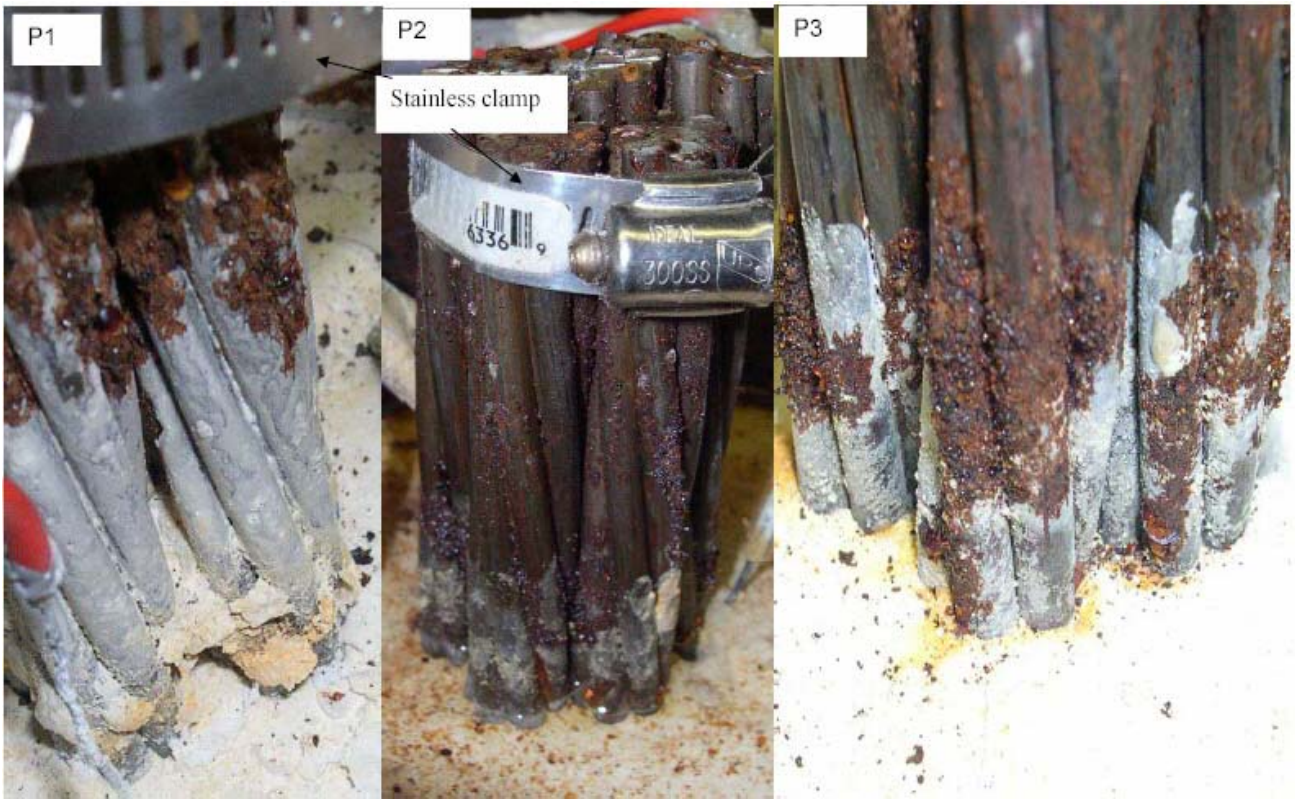

Figure 6. Corrosion on strands in P series assemblies at day 308 (after three water recharge events). Severe air space corrosion on all three bundles. Slight grout/void interface corrosion in P3. White grout residues left by bleed water.

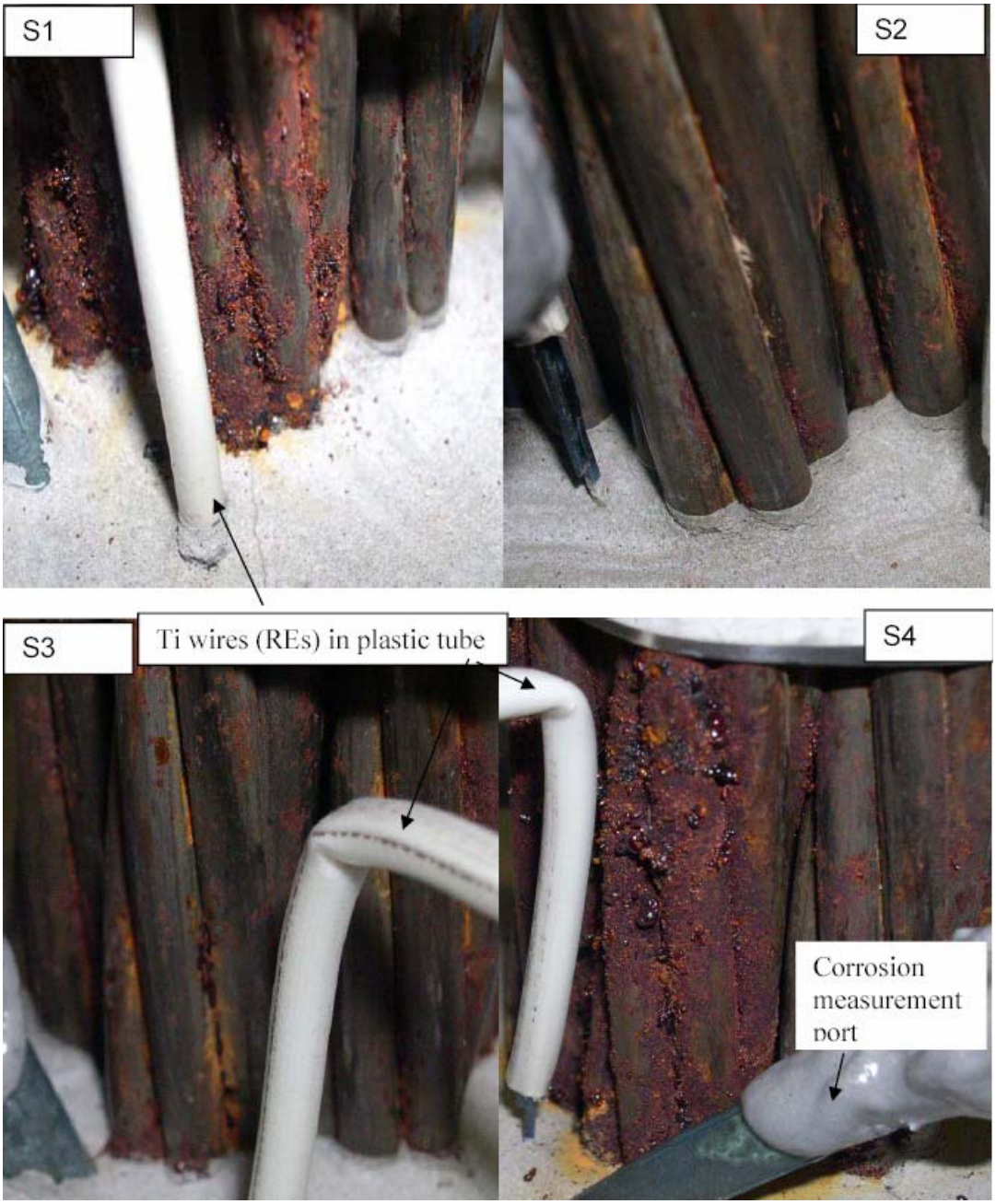

Figure 7. Corrosion on PT strands In S series assemblies (Day 272)
(S1, S3, and S4 showed corrosion attack at the grout/void interface; S2 showed almost no corrosion attack.)

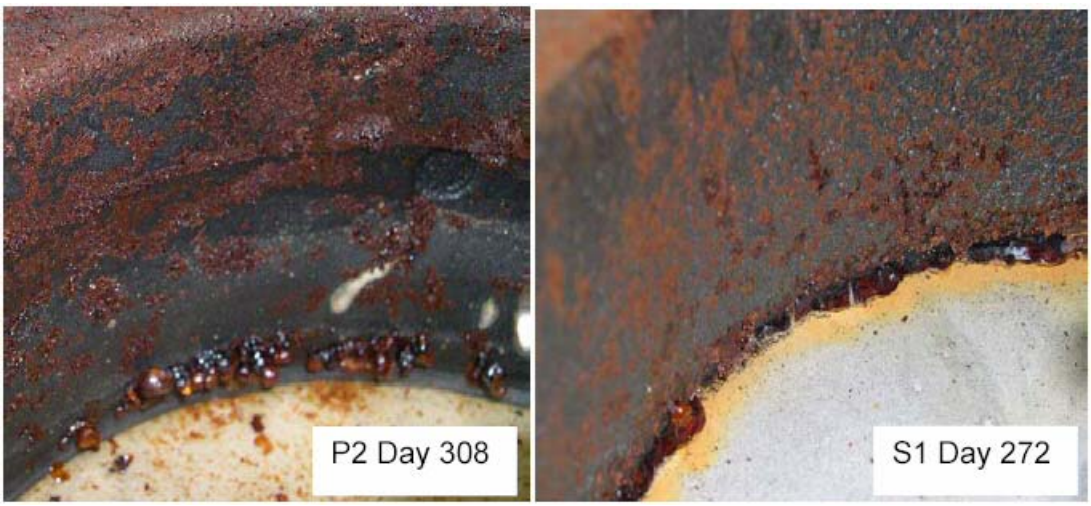

Figure 8. Corrosion on anchor body.
a: severe water line corrosion in P assembly after 0.01N NaCl recharge,
b: water line corrosion attack in S assembly after fresh water recharge.

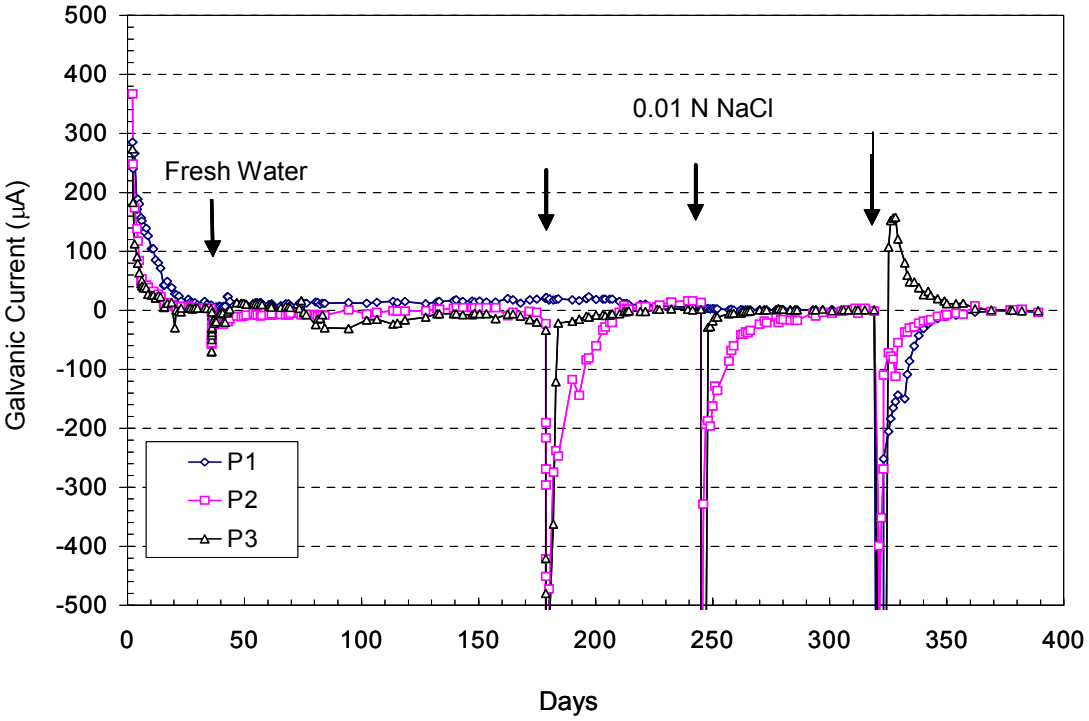

Figure 9. Galvanic current between anchor and strands in P series assemblies (arrows present the water recharge events listed in the test matrix; negative current sign indicates that strands serve as the cathodes)

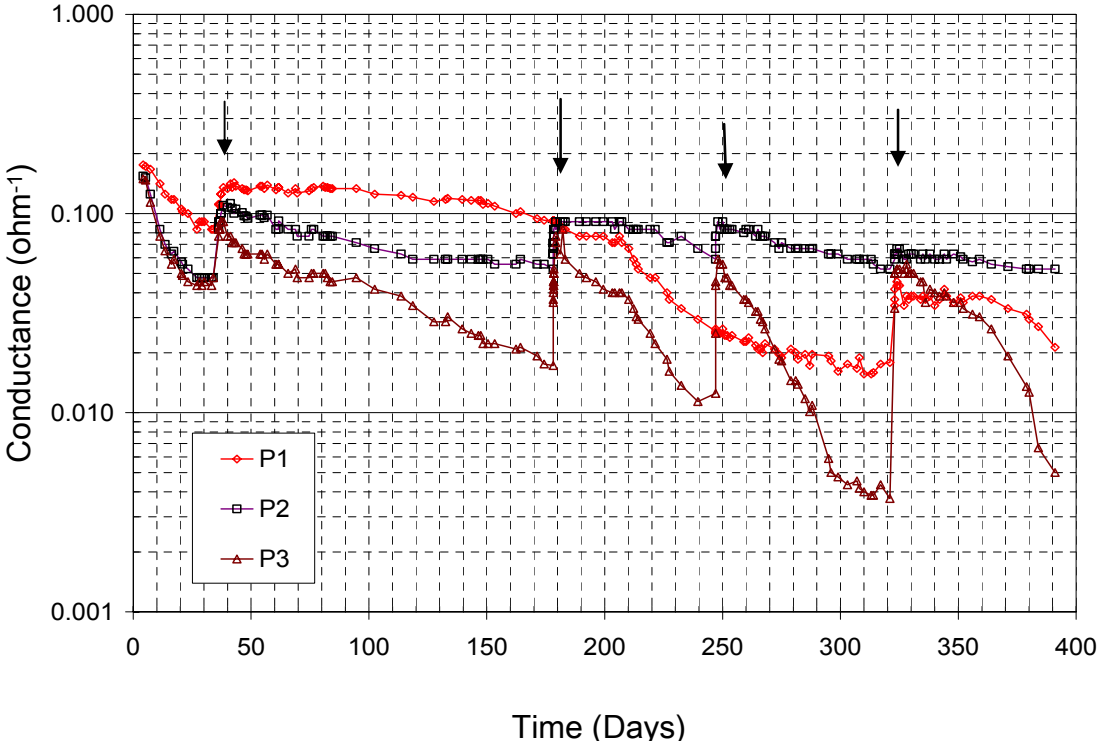

Figure 10. Conductance between anchor and strands in P series assemblies (arrows present the water recharge events listed in the test matrix)

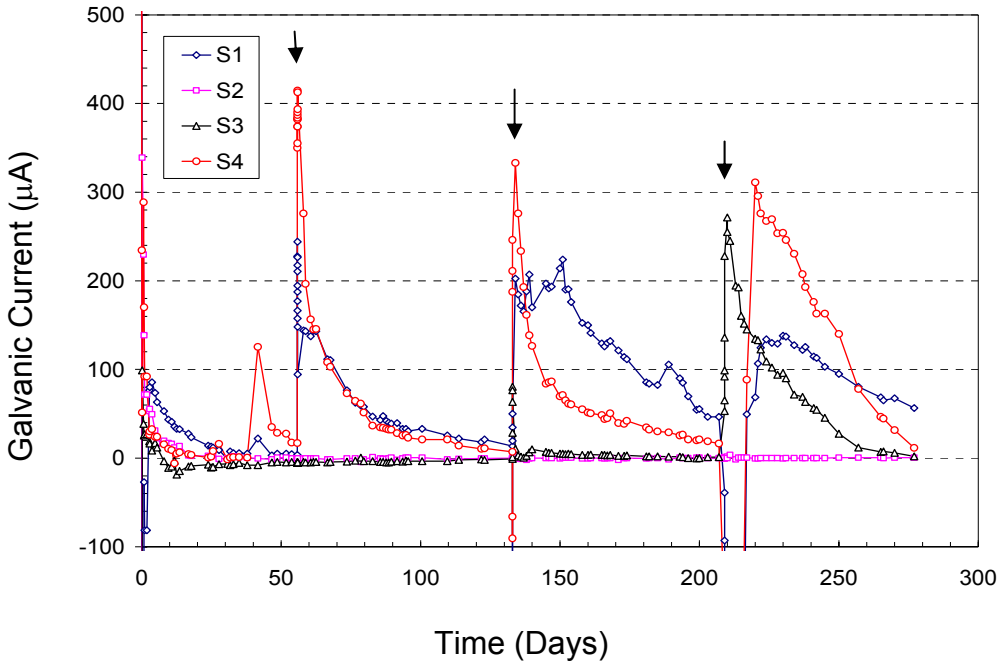

Figure 11. Galvanic current between anchor and strands in S series assemblies (arrows present the water recharge events listed in the test matrix; positive current sign indicates that strands serve as the anodes).

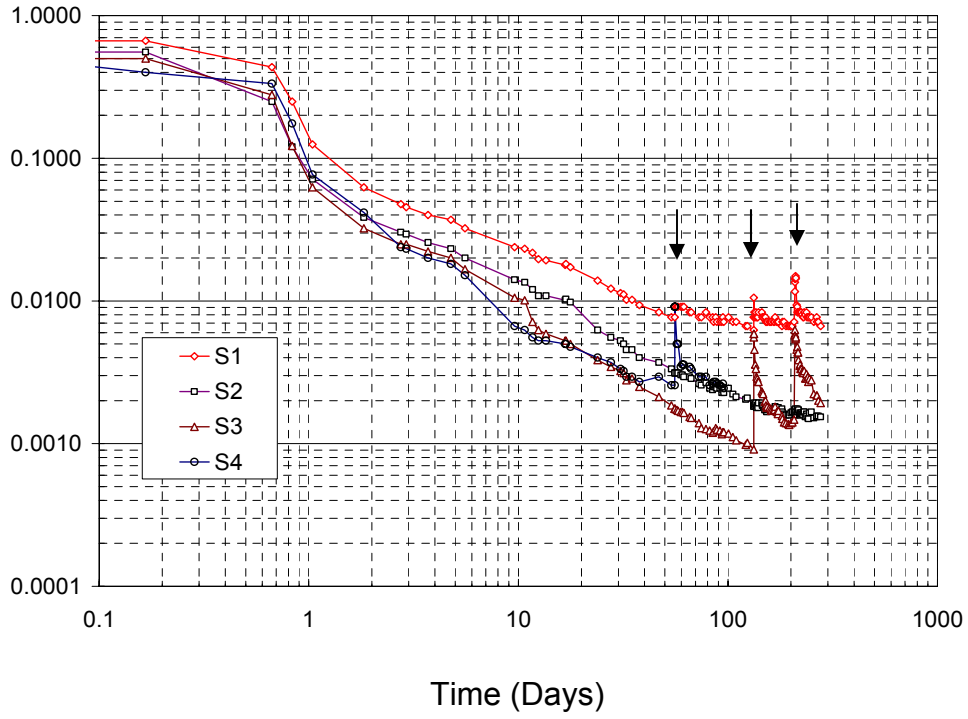

Figure 12. Conductance between anchor and strands in S series assemblies (arrows denote the water recharge events listed in the test matrix).

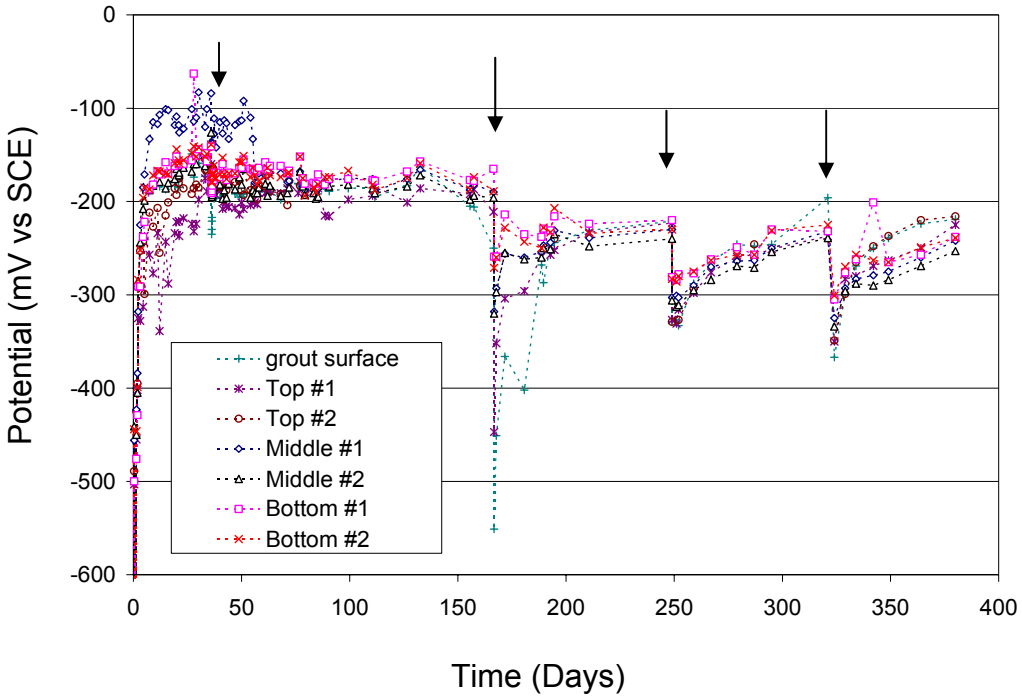

Figure 13. Potential change of the anchor-strands system with time for the P2 assembly (arrows represent the water recharge events listed in the test matrix; locations for potential readings measured at top, middle and bottom listed as 5-1,2,3 in fig. 3).

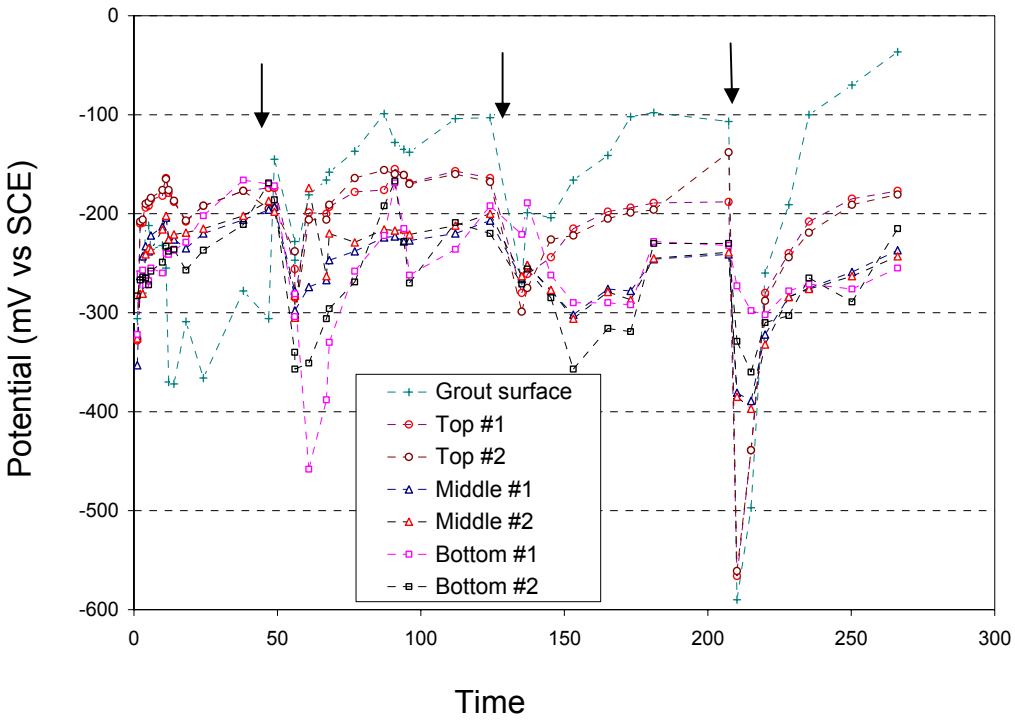

Figure 14. Potential change of the anchor-strands system with time for the S1 assembly (arrows present the water recharge events); locations for potential readings measured at the top, middle and bottom locations (Figure 3).

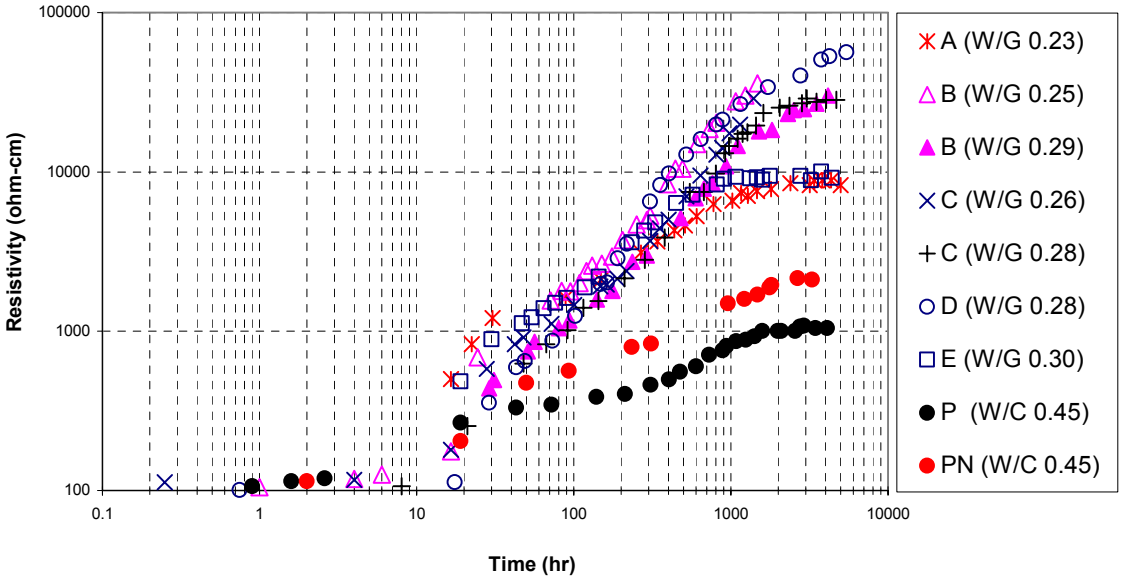

Figure 15. Grout resistivity as function of curing time in sealed containers. W/C, W/G indicates water to cement or grout ratio respectively of individual specimens of a given type.

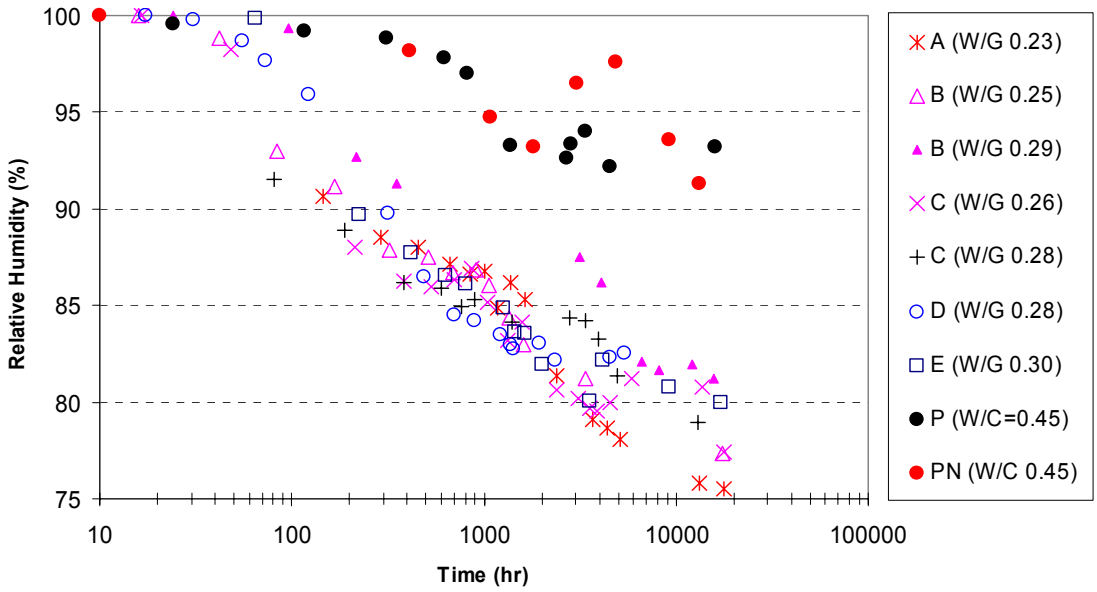

Figure 16. Internal relative humidity as function of curing time in sealed containers. W/C, W/G indicates water to cement or grout ratio respectively of individual specimens of a given type.

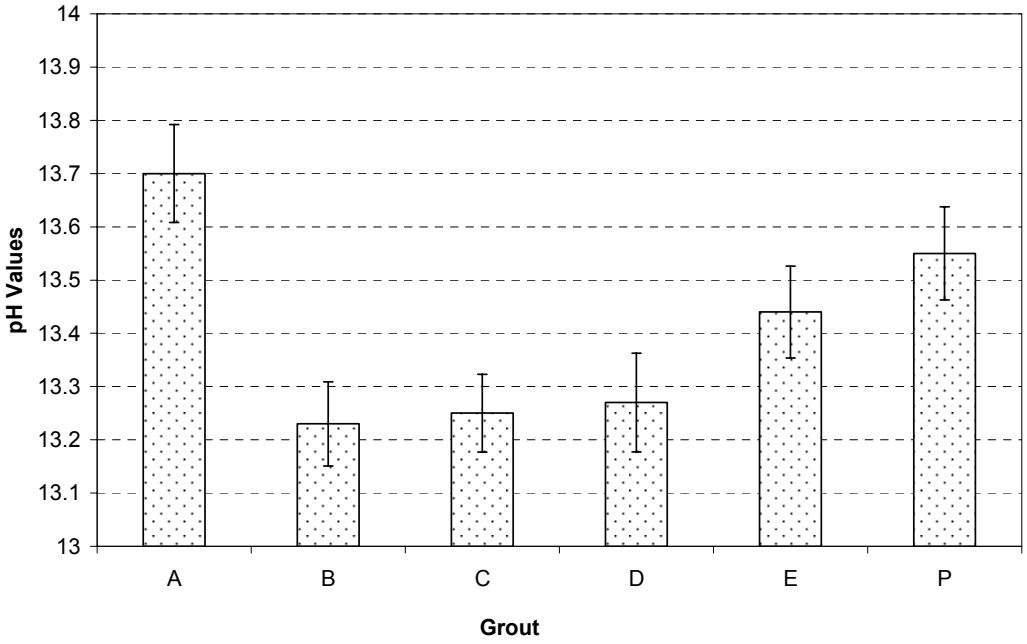

Fgure 17. Result of ISL measurements of grout pore water pH. Stabilization time > 100 days. Range of results is shown for tests where multiple measurements are available.

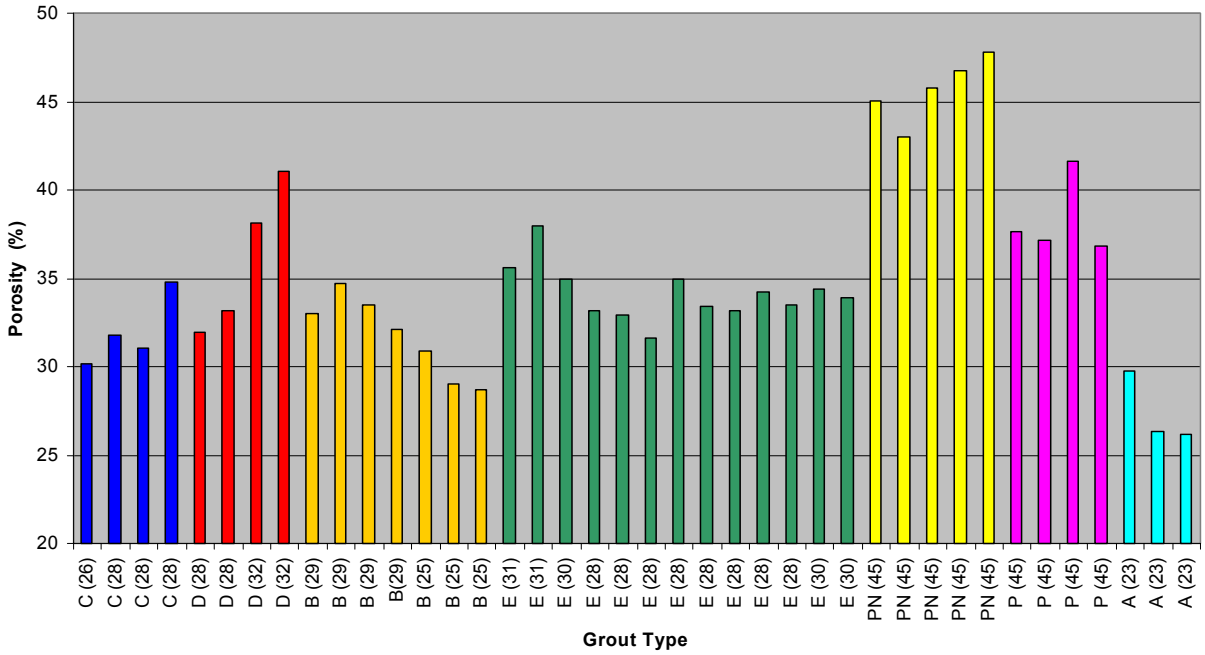

Figure 18. Results of porosity measurements. The value in parenthesis denotes W/C or W/G (x 100) of the particular grout tested.

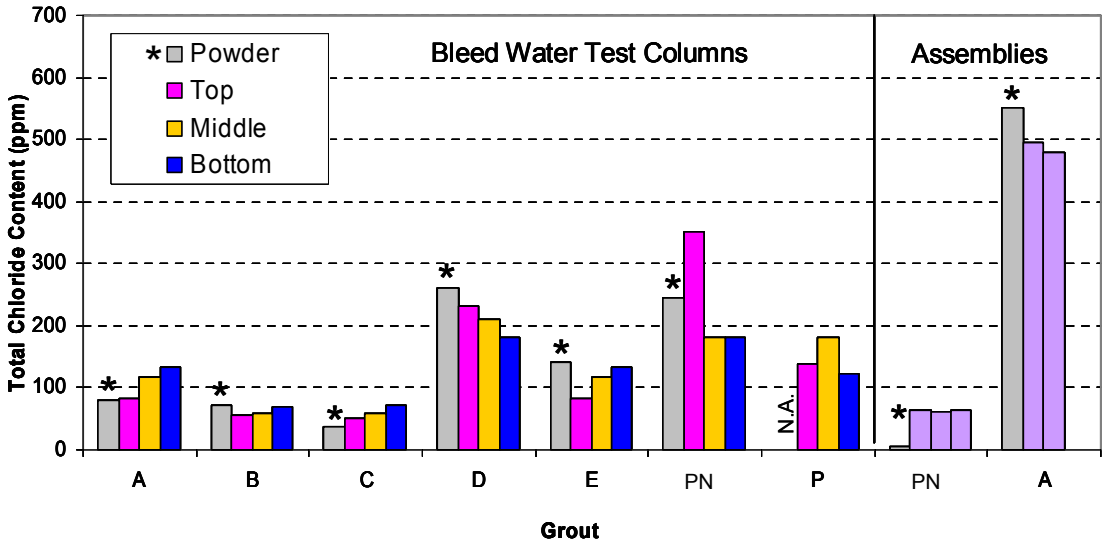

Figure 19 Chloride content as ppm of dry weight of grout or cement base stock powder (asterisk; N.A. not available), and of hardened grout extracted from bleed water test columns or from top surface of grout in mock-up assemblies. PN and A are from P and S assemblies respectively. Deionized water was used for all mixes.

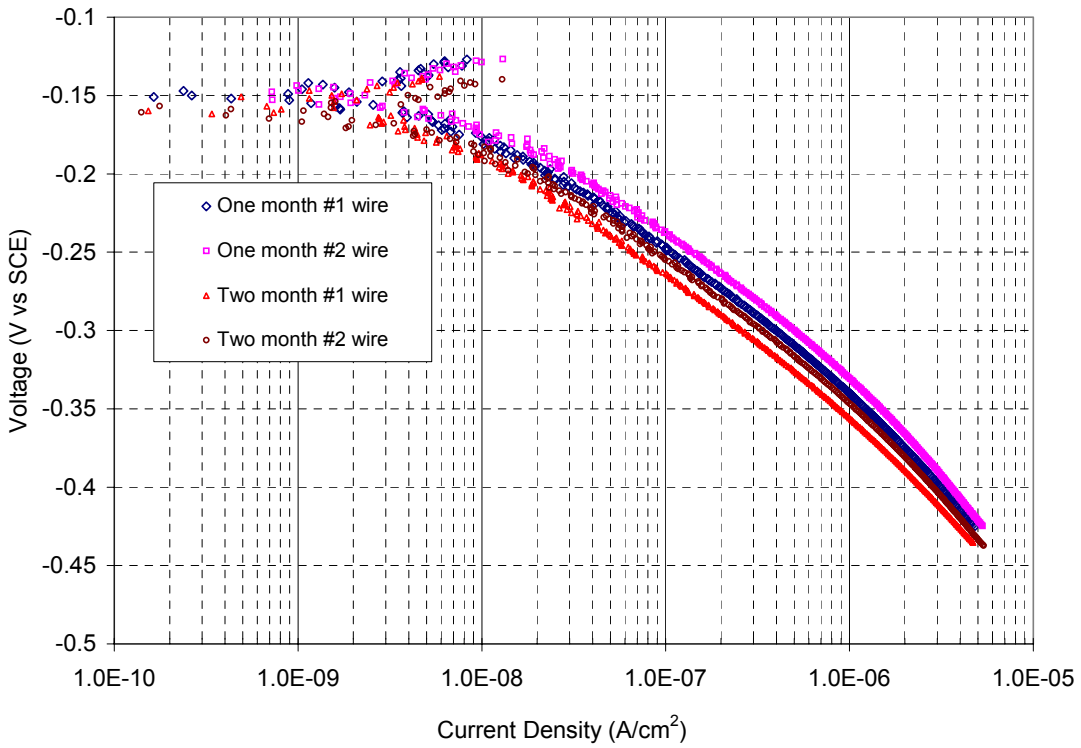

FIGURE 20. Oxygen reduction polarization of 0.2" Post-Tensioning Wire (SCS, scan rate=0.167 mV/s, open to air)

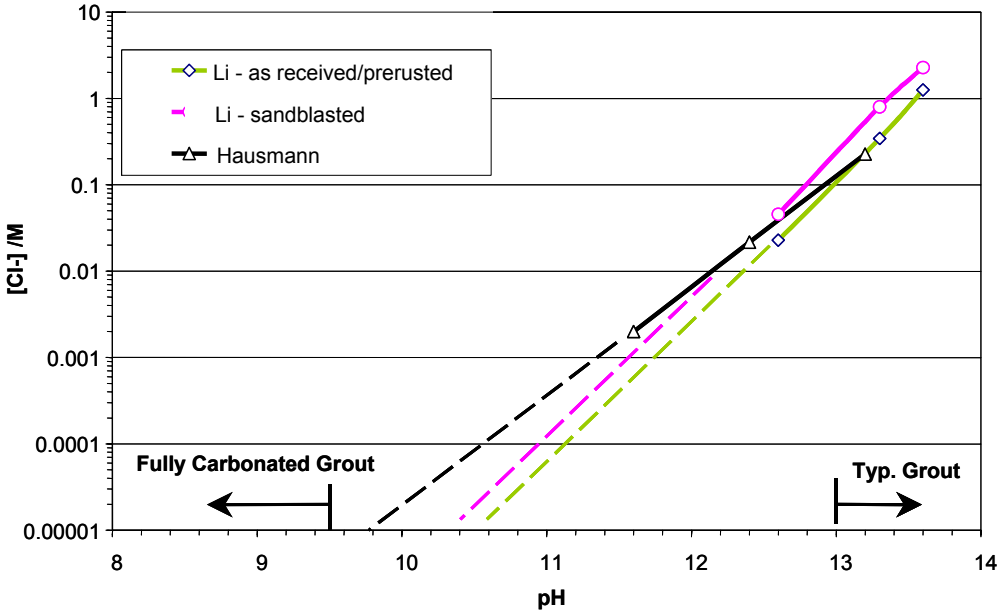

Figure 21. Chloride concentration threshold to initiate corrosion as function of pH for rebar steel (data from Hausmann and Li, see text).

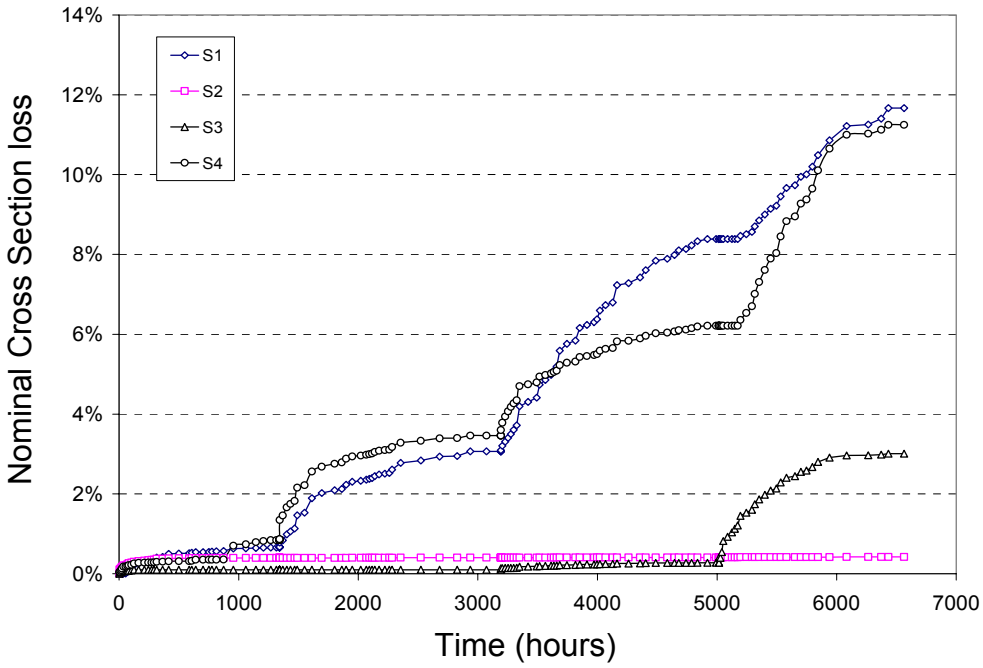

Figure. 22. Nominal cross section loss of a single strand. see text for assumptions used.

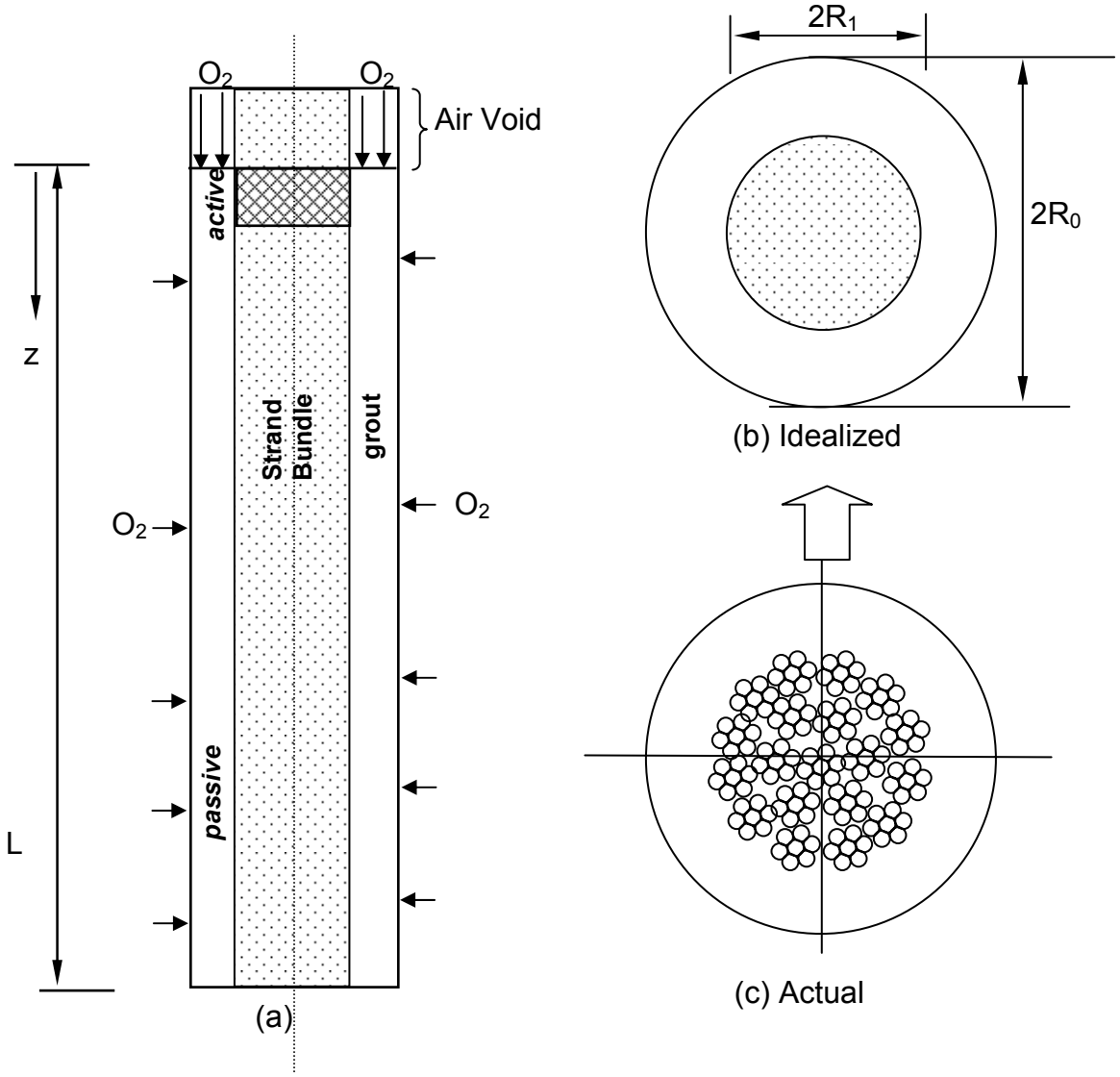

Figure 23. Schematic of a simple grout-strand cylinder system (strands encased in HDPE duct)

(a) Longitudinal cross section.
(b) Transversal cross-section.
(c) 19 7-wire strands in the HDPE duct, simplified to one nominal cylinder surface in (a) and (b).

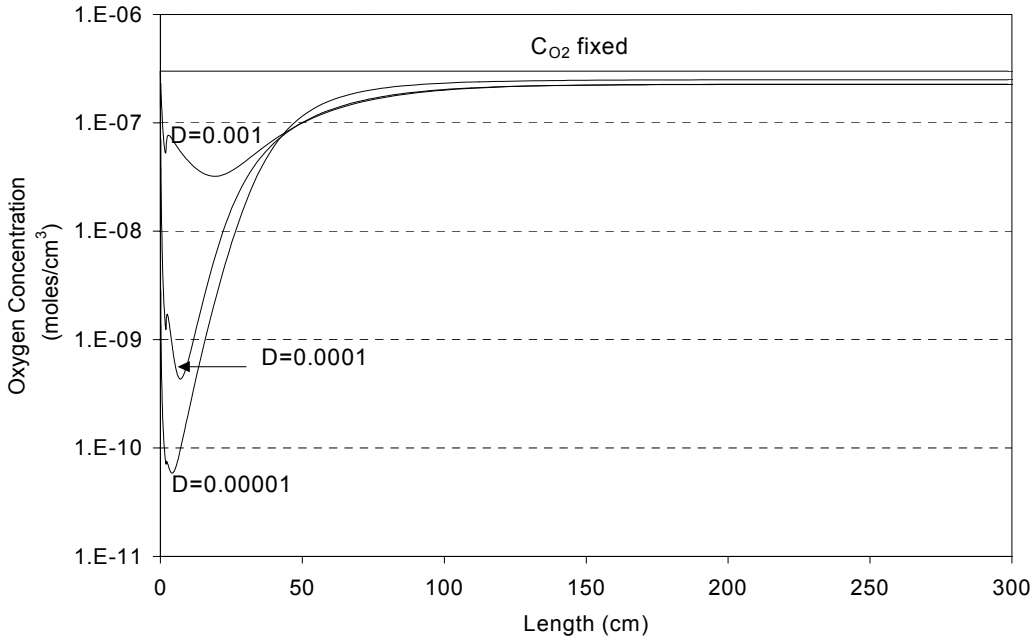

Figure 24. Longitudinal distribution of oxygen on the grout next to the strand surface (Resistivity=10^4 Ohm-cm). Values of oxygen diffusivity, D, for the case A series are in cm^2/sec. C_{O2} is fixed for the case B series.

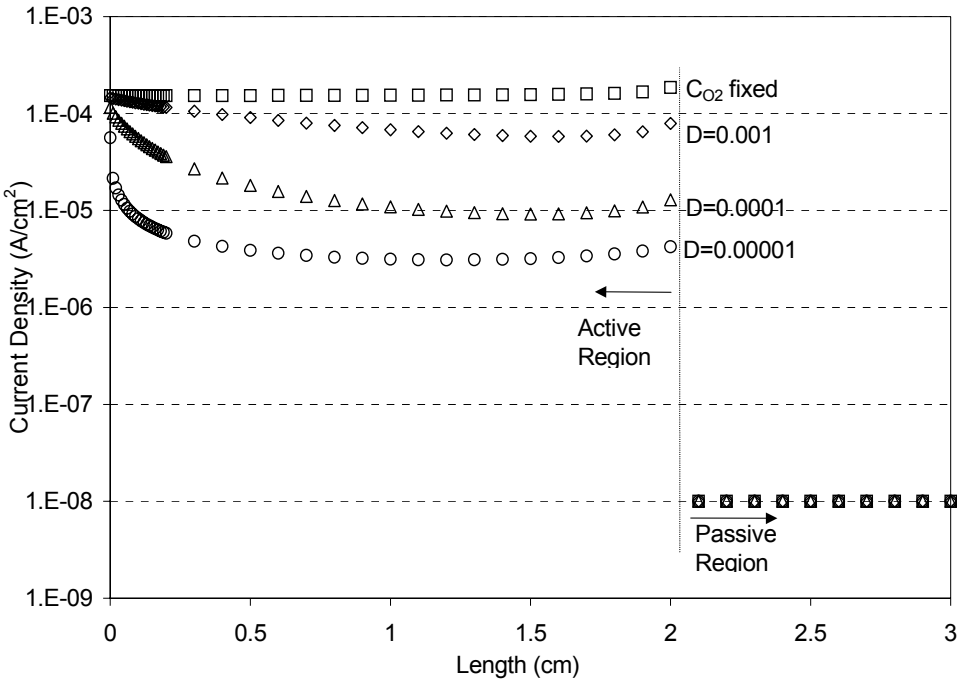

Figure 25. Longitudinal distribution of anodic current density (Region near active spot, Resistivity=10^4 Ohm-cm). Values of oxygen diffusivity, D, for the case A series are in cm^2/sec. C_{O2} is fixed for the case B series.

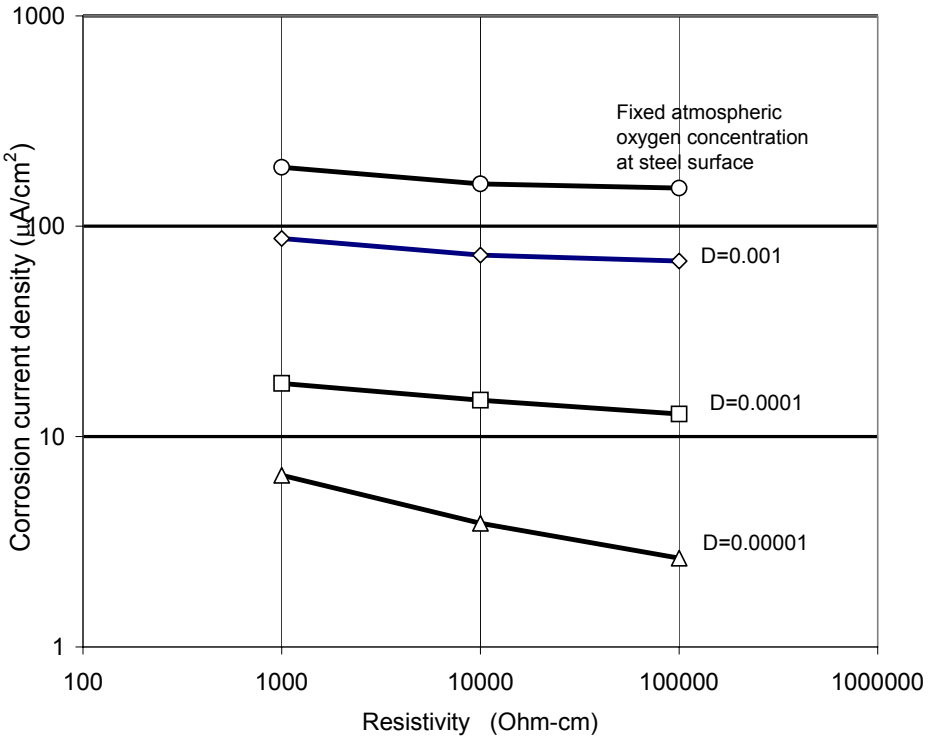

Figure 26. Average corrosion rate of the anodic zone as function of grout resistivity and oxygen diffusivity (Case A series), and for free oxygen transport to the steel surface (Case B series). Values of oxygen diffusivity, D, for the case A series are in cm^2/sec.

UNIT CONVERSIONS TABLE

CONVERSION FACTORS, US CUSTOMARY TO METRIC UNITS

Multiply	***by***	***to obtain***
inch	25.4	mm
foot	0.3048	meter
square inches	645	square mm
cubic yard	0.765	cubic meter
pound/cubic yard	0.593	kg/cubic meter
$inch^2$/year	$2.046\ 10^{-7}$	cm^2/sec
gallon/cubic yard	4.95	liter/cubic meter
standard cubic feet/hour	466.67	ml/minute
ounces	28.35	gram
pound	0.454	kilogram
pound (lb)	4.448	newtons
kip (1000 lb)	4.448	kilo newton (kN)
kilo newton (kN)	0.22481	kip (1000 lb)
pound/in^2	0.0069	MPa
kip/in^2	6.895	MPa
ft-kip	1.356	kN-m
in-kip	0.113	kN-m